Multifunctional organometallic compounds for the treatment of Chagas Disease: Re(I) tricarbonyl compounds with two different bioactive ligands

Mariano Soba, Gonzalo Scalese, Federico Casuriaga, Nicolás Pérez, Nicolás Veiga, Gustavo Etcheverria, Oscar Enrique Piro, Ricardo Faccio, Leticia Pérez-Díaz, Gilles Gasser, et al.

Multifunctional organometallic compounds for the treatment of Chagas Disease: Re(I) tricarbonyl compounds with two different bioactive ligands

Mariano Soba[1,2], Gonzalo Scalese[1], Federico Casuriaga[1], Nicolás Pérez[1], Nicolás Veiga[1], Gustavo A. Echeverría[3], Oscar E. Piro[3], Ricardo Faccio[4], Leticia Pérez-Díaz[5], Gilles Gasser[6], Ignacio Machado[7]*, Dinorah Gambino[1]*

[1]*Área Química Inorgánica, DEC, Facultad de Química, Universidad de la República, Uruguay*

[2]*Programa de Posgrado en Química, Facultad de Química, Universidad de la República, Montevideo, Uruguay*

[3]*Departamento de Física, Facultad de Ciencias Exactas, Universidad Nacional de La Plata and Institute IFLP (CONICET, CCT-La Plata), La Plata, Argentina*

[4]*Área Física, DETEMA, Facultad de Química, Universidad de la República, Uruguay*

[5]*Laboratorio de Interacciones Moleculares, Facultad de Ciencias, Universidad de la República, Uruguay*

[6]*Chimie ParisTech, PSL University, CNRS, Institute of Chemistry for Life and Health Sciences, Laboratory for Inorganic Chemical Biology, France.*

[7]*Área Química Analítica, DEC, Facultad de Química, Universidad de la República, Uruguay*

* To whom correspondence should be addressed. E-mail: dgambino@fq.edu.uy; imachado@fq.edu.uy Tel. +5982-9249739; fax: +5982-9241906

Keywords: Chagas disease; clotrimazole; metals in medicine; multifunctional metal compounds; Re(I) complexes; *Trypanosoma cruzi*

Abstract

Chagas' disease (American Trypanosomiasis) is an ancient and endemic illness in Latin America caused by the protozoan parasite *Trypanosoma cruzi.* Although there is an urgent need for more efficient and less toxic chemotherapeutics, no new drugs to treat this disease have entered the clinic in the last decades. Searching for metal-based prospective antichagasic drugs, in this work, multifunctional Re(I) tricarbonyl compounds bearing two different bioactive ligands were designed: a polypyridyl NN derivative of 1,10-phenanthroline and a monodentate azole (Clotrimazole CTZ or Ketoconazol KTZ). Five *fac*-[$Re(CO)_3(NN)(CTZ)](PF_6)$ compounds and a *fac*-[$Re(CO)_3(NN)(KTZ)](PF_6)$ were synthesized and fully characterized. They showed activity against epimastigotes (IC_{50} 3.48–9.42 μM) and trypomastigotes of *T. cruzi* (IC_{50} 0.61–2.79 μM)) and moderate to good selectivity towards the parasite comparing to VERO mammalian cell model. In order to unravel the mechanism of action of our compounds, two potential targets were experimentally and theoretically studied, namely DNA and one of the enzymes involved in the parasite ergosterol biosynthetic pathway, CYP51 (lanosterol 14-α-demethylase). As hypothesized, the multifunctional compounds shared *in vitro* a similar mode of action as that disclosed for the single bioactive moieties included in the new chemical entities. Additionally, two relevant physicochemical properties of biological interest in prospective drugs development, namely lipophilicity and stability in solution in different media, were determined. The whole set of results demonstrates the potentiality of these Re(I) tricarbonyls as promising candidates for further antitrypanosomal drug development.

Introduction

Chagas' disease (American Trypanosomiasis) is an ancient and endemic illness in Latin America caused by the flagellated protozoan parasite *Trypanosoma cruzi* (*T. cruzi*). It is mainly transmitted to the mammalian host by infected blood-sucking triatomine bugs. The parasite shows a complex life cycle that involves stages in the host (motile infective trypomastigotes and intracellular replicative amastigotes) and in the infected insect (non-replicative metacyclic trypomastigotes and non-infective epimastigotes) that show different susceptibility to drugs. In Latin America and the Caribbean region, there are about 8 million infected people, 10,000 annual deaths and 25 million people at risk of infection and the burden of the disease is five times higher than that of malaria. Migration flow towards North America, Australia, Europe and Japan, has led, in the last decades, to an increased number of cases in these non-endemic regions due to non-bug associated transmission ways, like blood transfusions, organ transplants and transmission from infected mother to newborn.[1-4] Chagas disease is classified as a neglected tropical disease by the World Health Organization, mainly due to low pharmaceutical industry investment in drug research associated to the low expected revenue. Consequently, most of the efforts related to the search of new chemotherapeutics have come from academy.[5-9]

Available chemotherapy is based on Benznidazole and Nifurtimox, two drugs developed more than 60 years ago, which proved to be toxic and to show low efficacy in the chronic stage of the disease and require long treatments that often develop drug resistance. Even though in the last years public-private efforts have pushed forward the drug discovery process, no new drugs to treat this disease have entered the clinic in the last decades.[10]

Consequently, there is an urgent need of new more efficient and less toxic chemotherapeutics for this disease.

In this context, the rational design of metal-based drugs including different metal ions or organometallic centers has shown to be a successful strategy for the development of new prospective agents against *T. cruzi*.[11-22]

The current working strategy of our group to obtain new metal-based antiparasitic compounds with improved biological profiles is based on the rational design of multifunctional metal compounds through molecular hybridization of different pharmacophoric moieties to produce an hybrid compound.[23-25] This design strategy involves the inclusion in a single chemical entity of a bioactive or pharmacologically relevant metal center, a bioactive ligand, i.e. an organic compound that had shown to have the desired activity, and, in some cases, a bioactive co-ligand. This approach has led in many cases to multifunctional compounds showing multiple modes of action and, additionally, to reduced toxicity and favorably modified selectivity profile.[11-14]

In this work, we report on the rational design of multifunctional Re(I) tricarbonyl compounds with two different bioactive ligands as prospective antichagasic agents: a polypyridyl NN derivative of 1,10-phenanthroline and a monodentate azole (Fig. 1).

Re(I) tricarbonyl compounds have demonstrated several advantages for medicinal chemistry purposes. The *fac*-$[Re(I)(CO)_3]^+$ center is chemically robust and easily accessible through a simple sequence of synthetic steps.[26] They have been successfully investigated in cancer therapy and as therapeutics in nuclear medicine.[27-31] This organometallic center has been described in antiparasitic compounds almost only as cyrhetrenyl derivatives.[32] Our group has reported some earlier promising results on *T. cruzi* of Re(I) tricarbonyls of bioactive semicarbazones and thiosemicarbazones.[33-34]

About the bioactive ligands, polypyridyl derivatives of 1,10-phenanthroline and their metal complexes have shown biological activity. In particular, most of the selected bidentate NN ligands have shown activity on *T. cruzi* (Fig. 1). Intercalating ability of these ligands may be transferred to the complexes, leading to DNA as a potential molecular target.[35-37]

On the other hand, the selected azoles have shown a potent antifungal and antiprotozoal activity acting on the ergosterol biosynthetic pathway. Ergosterol is the main sterol in trypanosomatid parasites and it is essential for providing structure and function of membranes and for parasite replication. Biosynthesis of ergosterol is a complicated parasite pathway involving several steps that differ from those of the human host. Therefore, it is a validated molecular target. Selected azoles inhibit the activity of lanosterol 14-alpha-demethylase (CYP51), enzyme that converts lanosterol in zymosterol, the precursor of ergosterol.[38]

Pioneering work by Sánchez-Delgado and his group has led to the development of classical coordination compounds and organometallics of Clotrimazole (CTZ) and Ketoconazol (KTZ) with different metals that showed interesting biological properties on *T. cruzi*. These promising results triggered the research of several groups around the world on metal compounds of these azole monodentate ligands.[13,14,18,39,40] Additionally, related Mn(I) tricarbonyls with some of the selected ligands have been successfully developed and tested on other trypanosomatid parasites and more recently on bacteria.[41,42]

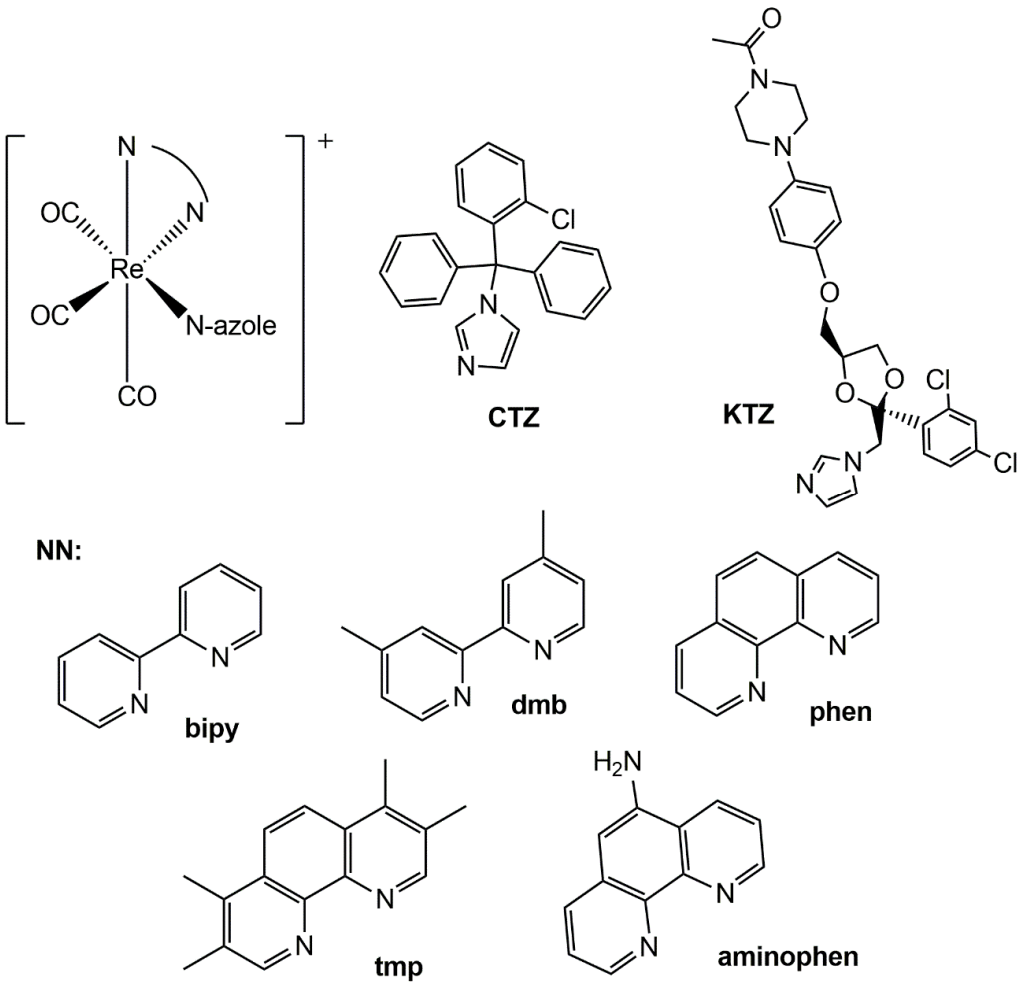

Fig 1. Structures of rationally designed *fac*-[Re(CO)$_3$(NN)(*N*-azole)](PF$_6$) where: *N*-azole is Clotrimazole (CTZ) or Ketoconazole (KTZ) and NN is a polypyridyl derivative of 1,10-phenanthroline. bipy: 2,2′-bipyridine; dmb: 4,4′-dimethyl 2,2′-bipyridine; phen: 1,10-phenanthroline; tmp: 3,4,7,8-tetramethyl-1,10-phenanthroline; aminophen: 5-amino-1,10-phenanthroline.

In summary, five new *fac*-[Re(CO)$_3$(NN)(CTZ)](PF$_6$) compounds, with the NN shown in Fig. 1, and *fac*-[Re(CO)$_3$(tmp)(KTZ)](PF$_6$) were synthesized and fully characterized. They were evaluated on epimastigotes and trypomastigotes of *T. cruzi* and on VERO cells as mammalian cell model. Distribution in *T. cruzi* epimastigotes was studied by Raman

Confocal Microscopy and compared with previously reported uptake and association to selected biomolecules fractions in the parasite determined by microwave plasma atomic emission spectrometry (MP-AES). To get insight into the probable mechanism of action of the compounds, interaction with DNA and inhibition of the biosynthesis of ergosterol have been experimentally and theoretically studied. Additionally, two relevant physicochemical properties of biological interest in prospective drugs development, namely lipophilicity and stability in solution in different media, were determined. The whole set of results emerging from this work demonstrates the potentiality of Re(I) tricarbonyl compounds as promising candidates for further antitrypanosomal drug development. Compounds bearing this metal center had remained almost unexplored for this medicinal chemistry application.

Experimental section

General considerations

All common laboratory chemicals were purchased from commercial sources and used without further purification.

Chemical and Physical Measurements

C, H and N analyses were performed with a Thermo Scientific Flash 2000 elemental analyzer. Rhenium was determined by microwave plasma atomic emission spectrometry (MP-AES) with an Agilent 4210 spectrometer, equipped with an inert One Neb nebulizer with a double-pass glass cyclonic spray chamber system, and an Agilent 4107 online nitrogen generator. Plasma gas flow was fixed at 20 L min^{-1} and auxiliary gas flow was fixed at 1.5 L min^{-1}. The analytical line was 346.046 nm.[43] FTIR spectra (4000 - 400 cm^{-}

[1]) were measured as KBr pellets with a Shimadzu IR Prestige-21 instrument. ^{1}H NMR spectra were recorded in DMSO-d_6 at 25ºC on a Bruker Avance NEO DPX-400 instrument. Homo-nuclear correlation spectroscopy (COSY) and hetero-nuclear single quantum coherence (HSQC) experiments were carried out with the same instrument. Residual peaks of DMSO were used as the internal standard and chemical shifts are reported in ppm.

Syntheses of the *fac*-[Re(CO)$_3$(NN)(*N*-azole)]PF$_6$ complexes

The complexes were synthesized through a general three-steps synthetic procedure shown in Fig. 2. The procedure follows modifications of previously described preparation of Re(I) tricarbonyls including other monodentate ligands.[44]

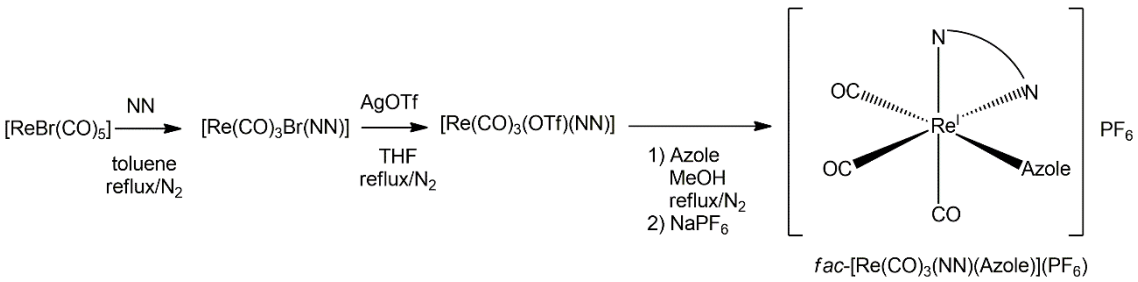

Fig 2. Scheme of synthesis of the [Re(CO)$_3$(NN)(*N*-azole)](PF$_6$) compounds. AgOTf = silver triflate.

All the reactions were performed under N_2 atmosphere and strictly protected from light. Briefly, [Re(I)(CO)$_5$Br] (50 mg, 0.123 mmol) and an equimolar amount of NN ligand (0.123 mmol) were suspended in 6 mL of toluene. The suspension was heated at reflux for 24 h. After cooling to room temperature, the obtained solid was washed twice with 2 mL portions of toluene and then left to dry in a vacuum desiccator for 24 h, protected from light. The dry solid and an equimolar amount of silver triflate, AgOTf, (32 mg, 0.123 mmol) were suspended in 7 mL of THF. The suspension was heated at reflux for 24 h.

The obtained suspension, containing AgBr precipitate, was centrifuged and the supernatant was removed. Afterwards, it was evaporated under reduced pressure and then resuspended in 5 mL of methanol. Subsequently, an equimolar amount of the azole (0.123 mmol) dissolved in 5 mL of methanol was added. The suspension was heated at reflux for 24 h. Once the reaction was completed, the obtained solution was reduced in volume to 5 mL by thermal evaporation. Finally, an equimolar amount of $NaPF_6$ (21 mg, 0.123 mmol) was added to the suspension and the mixture was stirred, protected from light, until a precipitate appeared. The obtained solid was separated by centrifugation, washed twice with 2 mL portions of ethanol, and placed in a vacuum desiccator for 24 h protected from light.

Synthesis of *fac*-[Re(CO)$_3$(phen)(CTZ)](PF$_6$)

A yellow solid was obtained. Yield: 46.0 mg (0.049 mmol), 40%. Anal. calc. for $C_{37}H_{25}ClF_6N_4O_3PRe$: C, 47.26; H, 2.68; N, 5.96 %. Found: C, 46.95, H, 2.54; N, 6.04 %. % Re: Anal. calc. 19.8 Found: 19.5. FTIR (KBr/cm^{-1}): 2030, 1943, 1915 ν(C≡O), 1586, 1561, 1495, 1444, 1429 ν(C=N), ν(C=C), 838 ν(P–F), 557 δ(F-P-F). ^{1}H-RMN (400 MHz, DMSO-d6): δ 9.55 (dd, *J* = 5.1, 1.4 Hz, 2H, H_{18}), 8.98 (dd, *J* = 8.3, 1.4 Hz, 2H, H_{20}), 8.32 (s, 2H, H_{21}), 8.06 (dd, *J* = 8.3, 5.1 Hz, 2H, H_{19}), 7.41 (td, *J* = 7.7, 1.6 Hz, 1H, H_{17}), 7.37 – 7.30 (m, 2H, H_{14}, H_{16}), 7.29 – 7.16 (m, 6H, H_4, H_6, H_8, H_9, H_{11}, H_{13}), 7.10 (m, 1H, H_1), 6.88 (m, 1H, H_2), 6.57 – 6.53 (m, 6H, H_3, H_5, H_7, H_{10}, H_{12}, H_{15}).

Synthesis of *fac*-[Re(CO)$_3$(aminophen)(CTZ)](PF$_6$)

An orange solid was obtained. Yield: 28.2 mg (0.030 mmol), 24 %. Anal. calc. for $C_{37}H_{29}ClF_6N_5O_3PRe$: C, 46.52; H, 2.74; N, 7.33 %. Found: C, 46.71; H, 2.47; N, 7.08 %. % Re: Anal. calc. 19.5 Found: 19.0. FTIR (KBr/cm^{-1}): 2030, 1915 ν(C≡O) (two

overlapped bands), 1597, 1560, 1493, 1448, 1432 ν(C=N), ν(C=C), 843 ν(P–F), 558 δ(F-P-F). ^{1}H-RMN (400 MHz, DMSO-d6): δ 9.48 (dd, *J* = 5.1, 1.2 Hz, 1H, H_{18}), 9.10 (dd, *J* = 8.6, 1.3 Hz, 1H, H_{19}), 9.02 (dd, *J* = 5.0, 1.2 Hz, 1H, H_{22}), 8.48 (dd, *J* = 8.5, 1.2 Hz, 1H, H_{23}), 8.00 (dd, *J* = 8.5, 5.1 Hz, 1H, H_{20}), 7.73 (dd, *J* = 8.4, 5.0 Hz, 2H, H_{21}), 7.43 (td, *J* = 7.7, 1.6 Hz, 1H, H_{17}), 7.37 – 7.21 (m, 9H, H_4, H_6, H_8, H_9, H_{11}, H_{13}, H_{14}, H_{16}, H_{24}), 7.10 (t, *J* = 1.6 Hz, 1H, H_1), 7.00 (m, 2H, H_{25}, H_{26}), 6.89 (m, 1H, H_2), 6.60 – 6.54 (m, 5H, H_5, H_7, H_{10}, H_{12}, H_{15}), 6.47 (m, 1H, H_3)

Synthesis of *fac*-[Re(CO)$_3$(bipy)(CTZ)](PF$_6$)

The solid was purified by means of a silica gel column, using a mixture MeOH:CH_2Cl_2 (20:80) as mobile phase. The first 20 mL of eluate were evaporated under reduced pressure and suspended in 10 mL of methanol. Subsequently, the complex was precipitated by dropwise addition of 10 mL of hexane. The obtained solid was washed with 1 mL of hexane and 1 mL of ethanol, and finally placed in a vacuum desiccator for 24 h protected from light. A yellow solid was obtained. Yield: 47.0 mg (0.051 mmol), 42 %. Anal. calc. for $C_{35}H_{25}ClF_6N_4O_3PRe$: C, 45.88; H, 2.75; N, 6.11%. Found: C, 46.22; H, 2.80; N, 6.13%. % Re: Anal. calc. 20.3 Found: 20.5. FTIR (KBr/cm^{-1}): 2030, 1941, 1917 ν(C≡O), 1604, 1560, 1491, 1444, 1433 ν(C=N), ν(C=C), 840 ν(P–F), 557 δ(F-P-F). ^{1}H-RMN (400 MHz, DMSO-d_6): δ 9.13 (dd, *J* = 5.5, 1.4 Hz, 2H, H_{18}), 8.69 (d, *J* = 8,2 Hz, 2H, H_{21}), 8.34 (td, *J* = 7.9, 1.5 Hz, 2H, H_{20}), 7.78 – 7.69 (m, 2H, H_{19}), 7.47 (td, *J* = 7.7, 1.6 Hz, 1H, H_{17}), 7.40 – 7.32 (m, 8H, H_4, H_6, H_8, H_9, H_{11}, H_{13}, H_{14}, H_{16}), 7.06 (m, 1H, H_1), 7.01 (m, 1H, H_2), 6.83 (m, 1H, H_3), 6.76 – 6.71 (m, 5H, H_5, H_7, H_{10}, H_{12}, H_{15}).

Synthesis of *fac*-[Re(CO)$_3$(tmp)(CTZ)](PF$_6$)

A yellow solid was obtained. Yield: 43.0 mg (0.043 mmol), 53 %. Anal. calc. for $C_{41}H_{33}ClF_6N_4O_3PRe$: C, 49.92; H, 3.34; N, 5.62 %. Found: C, 49.33; H, 3.70; N, 5.59 %. % Re: Anal. calc. 18.7 Found: 18.3. FTIR (KBr/cm^{-1}): 2030, 1930, 1902 ν(C≡O), 1599, 1560, 1491, 1447, 1431 ν(C=N), ν(C=C), 842 ν(P–F), 558 δ(F-P-F). ^{1}H-RMN (400 MHz, DMSO-d_6): δ 8.28 (s, 2H, H_{19}), 8.39 (s, 2H, H_{24}), 7.43 (td, J = 7.7, 1.6 Hz, 1H, H_{17}), 7.31 – 6.19 (m, 8H, H_4, H_6, H_8, H_9, H_{11}, H_{13}, H_{14}, H_{16}), 7.10 (m, 1H, H_1), 6.90 (m, 1H, H_2), 6.75 (m, 1H, H_3), 6.66 (dd, J = 8.0, 1.6 Hz, 1H, H_{15}), 6.60 – 6.55 (m, 4H, H_5, H_7, H_{10}, H_{12}), 2.82 (s, 6H, H_{22}, H_{23}), 2.55 (s, 6H, H_{20}, H_{21}).

Synthesis of *fac*-[Re(CO)$_3$(dmb)(CTZ)](PF$_6$)

A yellow solid was obtained. Yield: 40.9 mg (0.043 mmol), 35 %. Anal. calc. for $C_{37}H_{29}ClF_6N_4O_3PRe$: C, 47.06; H, 3.10; N, 5.93 %. Found: C, 46.79; H, 3.68; N, 5.87 %. % Re: Anal. calc. 19.7 Found: 19.3. FTIR (KBr/cm^{-1}): 2035, 1919 ν(C≡O) (two overlapped bands), 1598, 1560, 1487, 1448, 1433 ν(C=N), ν(C=C), 840 ν(P–F), 557 δ(F-P-F). ^{1}H-RMN (400 MHz, DMSO-d_6): δ 8.93 (d, J = 5.7Hz, 2H, H_{18}), 8.55 (d, J = 1.8 Hz, 2H, H_{21}), 7.58-7.53 (m, 2H, H_{19}), 7.48 (td, J = 7.6, 1.6 Hz, 1H, H_{17}), 7.42 – 7.31 (m, 8H, H_4, H_6, H_8, H_9, H_{11}, H_{13}, H_{14}, H_{16}), 7.09 (m, 1H, H_1), 7.02 (m, 1H, H_2), 6.80 – 6.69 (m, 6H, H_3, H_5, H_7, H_{10}, H_{12}, H_{15}), 2.53 (s, 6H, H_{20}).

Synthesis of *fac*-[Re(CO)$_3$(tmp)(KTZ)](PF$_6$)

A brown solid was obtained. Yield: 85.0 mg (0.048 mmol), 69 %. Anal. calc. for $C_{45}H_{44}Cl_2F_6N_6O_7PRe$: C, 45.69; H, 3.75; N, 7.10%. Found: C, 45.12; H, 3.71; N, 6.97%. % Re: Anal. calc. 10.5. Found: 10.4. FTIR (KBr/cm^{-1}): 2031, 1914 ν(C≡O) (two overlapped bands), 1585, 1561, 1491, 1449, 1432 ν(C=N), ν(C=C), 844 ν(P–F), 557 δ(F-P-F).^{1}H-RMN (400 MHz, DMSO-d_6): δ 9.40 (d, J = 3.6Hz, 2H, H_{19}), 8.38 (m, 2H, H_{15}),

7.79 (d, *J* =1.4 Hz, 1H, H_6), 7.55 (m, 1H, H_1), 7.23 (dd, *J* = 8.5, 2.1 Hz, 1H, H_7), 7.10 (d, *J* = 8.5 Hz, 1H, H_8), 6.91 (d, *J* = 8.8 Hz, 2H, H_{14}), 6.85 (m, 1H, H_2), 6.63 (m, 1H, H_3), 6.61 (m, 2H, H_{24}), 4.33 (m, 2H, H_4, H_5), 4.08 (m, 1H, H_{11}), 3.58 (m, 5H, H_{13}, H_{16}), 3.23 (m, 2H, H_9, H_{12}), 3.02 (dt, *J* = 2.5, 5,2 Hz, 4H, H_{17}), 2.87 (dd, *J* = 8.3, 5.8 Hz, 1H, H_{10}), 2.82 (s, 3H, H_{22}), 2.74 (s, 3H, H_{23}), 2.65 (s, 3H, H_{20}), 2.63 (s, 3H, H_{21}), 2.05 (s, 3H, H_{18}).

X-ray diffraction study of *fac*-[Re(CO)$_3$(phen)(CTZ)](PF$_6$)

Single crystals were obtained from methanol. The measurements were performed on an Oxford Xcalibur Gemini, Eos CCD diffractometer with graphite-monochromated MoKα (λ = 0.71073 Å) radiation. X-ray diffraction intensities were collected (ω scans with ϑ and κ-offsets), integrated and scaled with CrysAlisPro suite of programs.[45]

The unit cell parameters were obtained by least-squares refinement (based on the angular settings for all collected reflections with intensities larger than seven times the standard deviation of measurement errors) using CrysAlisPro. Data were corrected empirically for absorption employing the multi-scan method implemented in CrysAlisPro. The structures were solved by intrinsic phasing with SHELXT[46] and the molecular model refined by full-matrix least-squares procedure with SHELXL of the SHELX suite of programs.[47]

Two polymorphs were solved, one triclinic and the other one monoclinic with two independent molecules per asymmetric unit. The hexafluorophosphate anion in the triclinic polymorph showed severe disorder which could not be satisfactorily modeled and therefore we proceeded with the further refinement of the more ordered part of the structure, *fac*-[Re(CO)$_3$(phen)(CTZ)]$^+$, resorting to a procedure described by van der Sluis and Spek[48] and implemented in the program SQUEEZE included in the PLATON suite of programs.[49] There resulted a void volume of 237 Å^3 per unit cell and a total

electron counting of 142 electrons/cell, in close agreement with expectations for the two PF_6 counterions in the unit cell.

Most H-atoms of both polymorphs were detected in difference Fourier maps phased on the heavier atoms. However, they were positioned on stereo-chemical basis and refined with the riding model. Crystal data and structure refinement results are summarized in Table S1. Crystallographic structural data have been deposited at the Cambridge Crystallographic Data Centre (CCDC). Any request to the Cambridge Crystallographic Data Centre for this material should quote the full literature citation and the reference numbers CCDC 1955911 [monoclinic] and CCDC 1955912 [triclinic].

Stability in solution

The chemical stability of the synthetized *fac*-[$Re(CO)_3$(NN)(CTZ)](PF_6) and *fac*-[$Re(CO)_3$(tmp)(KTZ)](PF_6) compounds was studied in solution using as solvents DMSO, DMSO:synthetic biological medium (50:50), DMSO:Brain Heart Infusion (BHI)-Tryptose supplemented with 10 % bovine serum (Sigma-Aldrich) medium (50:50) and DMSO:fetal bovine serum (Sigma-Aldrich) (50:50), employing reverse phase high performance liquid chromatography (RP-HPLC-DAD).[50]

The synthetic biological medium consisted of a mixture containing 2.5 g L^{-1} Na_2HPO_4, 5 g L^{-1} NaCl and 2 g L^{-1} glucose.[51] This composition was established to simulate the BHI culture medium in which the parasites were grown. A Shimadzu Prominence LC-20AT liquid chromatograph coupled to a Shimadzu PD-M20A diode array detector was used. An Agilent ZORBAX Eclipse Plus C18 column (4.6 × 100 mm; 3.6 μm), thermostated at 25 °C, was used as the stationary phase. A 40 mM phosphate buffer solution pH 7.4 (A) and MeOH (B) were used as mobile phases flowing at a constant flow rate of 1 mL min^{-1}, according to the gradient shown in Table S2.[50,52]

For the preparation of the solutions, 1.0 mg of each compound was dissolved in 2.0 mL of each media. Obtained solutions were filtered using 0.45 μm pore size PVDF transfer membranes. An injection volume of 50 μL was established per run. The wavelength used for monitoring was 250 nm, obtaining retention times (t_R) between 22 and 23 min for the studied compounds in all solvents. Stability was studied in a period of 5 days, for DMSO and DMSO: synthetic medium, being the solutions measured at t_1= 0 and t_2= 5 days, under the same chromatographic conditions. Similarly, the stability in supplemented BHI medium and in DMSO:fetal bovine serum (Sigma-Aldrich) (50:50), was studied over a period of 1 day, being the solutions measured at t_1= 0 and t_2= 1 day.

Stability in human plasma

The stability of *fac*-[$Re(CO)_3(NN)(CTZ)](PF_6)$ and *fac*-[$Re(CO)_3(tmp)(KTZ)](PF_6)$ compounds in human plasma was studied following a previously reported procedure.[50] Fresh 5.0 mM stock solutions were prepared in DMSO and ultrapure water for the compounds and caffeine (internal standard), respectively. An aliquot of 12.5 μL of the compound to be studied (from 5.0 mM stock solution) and 12.5 μL of caffeine stock solution were added to 975 μL of human plasma. The mixture was incubated for 0, 1, 3, 6, and 24 h at 37 °C with continuous and gentle shaking (700 rpm) while protected from light. After the incubation time, plasma solution was quenched with 1 mL of MeOH and 2 mL of dichloromethane (DCM), and the mixture was shaken for 30 min at room temperature. The resulting mixture was centrifuged at 6000 rpm for 10 min. The organic layer was separated from the aqueous layer and DCM was removed by means of a reduced pressure rotary evaporator. The residue was redissolved in CH_3CN and filtered using a 0.22 μm membrane filter. Stability of the compounds was monitored by reverse phase high performance liquid chromatography (RP-HPLC-DAD). An Agilent 1260 Infinity

liquid chromatograph coupled to a diode array detector was used. An Agilent Pursuit XRs 5 C18 column (4.6x250 mm, 5.0 μm) was employed as the stationary phase. A mixture of CH_3CN: water (90:10) was used as the mobile phase, flowing at a constant rate of 1.0 mL min^{-1} in isocratic mode. The injection volume was 25 μL. The monitoring wavelength was 270 nm.

Lipophilicity studies

Lipophilicity of *fac*-[$Re(CO)_3(NN)(CTZ)$](PF_6) compounds was studied in solution by reverse phase high performance liquid chromatography (RP-HPLC-DAD).[53,54]

A Shimadzu Prominence LC-20AT liquid chromatograph coupled to a Shimadzu SPD-M20A diode array detector was used. An Agilent ZORBAX Eclipse Plus C8 (4.6x250 mm, 5.0 μm) was employed as the stationary phase. A mixture of MeOH:40 mM phosphate buffer pH 7.4 (70:30) was used as the mobile phase, flowing at a constant rate of 0.8 mL min^{-1} in isocratic mode. The injection volume was 50 μL. The monitoring wavelength was 250 nm. Solutions were prepared by dissolving 1 mg of each compound in 2 mL of DMSO and were filtered using 0.45 μm pore size PVDF transfer membranes. Tartrazine was used for the estimation of the hold-up time (t_0). This compound is often used to estimate t_0 of a chromatographic column, since due to its polar properties it has little affinity for nonpolar stationary phases such as C8.[55]

Additionally, the lipophilicity of the complexes was experimentally determined by the *shake flask* method. Complexes were dissolved in a little amount of DMSO and subjected to an octanol-PBS previously saturated in each other (2-3 h of previous shaking), and shaked overnight. After that, the samples were settled 30 min and centrifugated 10 min at 6000 rpm. The organic layer was analyzed by UV-Vis spectroscopy in an Agilent Cary

UV-Vis Multicell Peltier and partition coefficient (logP) was determined as previously described.[56]

Calibration curves were made by adding incremental amounts of the compound in octanol using the maximum of the absorption spectra to build the curve.

Biological studies

In vitro activity on *T. cruzi* (Dm28c strain epimastigotes and CL Brener strain trypomastigotes) and cytotoxicity on mammalian cells (VERO cells)

Parasites experiments were carried out using *T. cruzi* epimastigotes (Dm28c strain) and trypomastigotes (CL Brener strain).

Dm28c epimastigotes were obtained from axenic cultures, maintained in exponential phase of growth by successive passages in Brain-heart infusion medium (BHI, Oxoid) supplemented with 10 % heat inactivated fetal bovine serum (FBS, Capricorn), penicillin (100 units/mL) and streptomycin (100 µg/mL) at 28 °C.

Cell derived trypomastigotes (CL Brener strain) were obtained from VERO cells infections. Metacyclic trypomastigotes were obtained from late stationary phase epimastigotes until a high proportion of metacyclic trypomastigote parasites were observed (~21 days). Metacyclic trypomastigote-rich cultures were incubated overnight with a monolayer of VERO cells in a 10:1 parasite:cell ratio in RPMI medium at 37°C in a humidified 5 % CO_2 incubator. Non invading extracellular parasites were removed the following day by washing the VERO cell monolayer three times with PBS, followed by addition of fresh complete RPMI supplemented with 10% FBS. Trypomastigotes emerged from VERO cells (6-7 days) were used to set new VERO cell infections up.[57]

Cell-derived trypomastigotes were obtained from the supernatant of infected VERO cells collected 72 h post established infection with cell-emerged trypomastigotes.

VERO cells. VERO cells (ATCC CCL81) were used as mammalian cell model for testing unspecific cytotoxicity. This cell lineage has been used as mammalian model in *Trypanosoma cruzi* infections.[58] Cells were cultured in RPMI medium (Gibco) supplemented with 10 % heat inactivated fetal bovine serum, penicillin (100 units/mL) and streptomycin (100 µg/mL) at 37°C in a humidified 5 % CO_2 incubator. For maintenance, confluent cells were washed with PBS, incubated for 3 min with trypsin-EDTA (Gibco), diluted and re-plated.[59]

Compounds´ treatment. The compounds were initially dissolved in DMSO (stock concentration). Freshly solutions were diluted in the culture medium to obtain the different concentrations tested. Throughout the experimental procedures, the concentration of DMSO never exceeded 1%, which is non-toxic for the protozoa.[59,60]

In vitro activity against epimastigotes of *T. cruzi*

$1x10^6$ parasites per well were seeded in black 96 well plates in BHI medium with increasing concentration of compounds for 24 h. A broad range of compound concentrations was tested for each compound to estimate the IC_{50} value (0-96 µM) and then this range was narrowed according to the calculated IC_{50} to reach an accurate value; particularly, 0-96 µM for $[Re(CO)_3(tmp)(KTZ)]PF_6$ complex, 0-144 µM for KTZ free ligand, 0-40 µM for bipy and dmb free ligands, 0-20 µM for CTZ, phen, tmp, $[Re(CO)_3(aminophen)(CTZ)]PF_6$ and $[Re(CO)_3(dmb)(CTZ)]PF_6$, 0-5 µM for aminophen, $[Re(CO)_3(phen)(CTZ)]PF_6$, $[Re(CO)_3(tmp)(CTZ)]PF_6$ and $[Re(CO)_3(bipy)(CTZ)]PF_6$. Viability was tested using alamar Blue™ (Thermo Fisher), where resazurin is reduced to resorufin, a compound that is red in color and highly fluorescent. Briefly, 24 h after

treatment, 10 µL of alamar Blue were added to each well and black plates were incubated for 3 h at 28°C. Fluorescence (excitation 530 nm / emission 590 nm) were measured in a Thermo Scientific Varioskan® Flash Multimode instrument. Dose-response curves were recorded and the IC_{50} values were determined using GraphPad Prism version 6.00 for Windows (GraphPad Software, La Jolla California USA). The results are presented as averages ± SD (standard deviation) of three independent biological replicates.[61] Nifurtimox (Nfx) was used as the reference anti-*T. cruzi* drug. Dose-response curves were recorded and the IC_{50} values were determined using GraphPad Prism version 6.00 for Windows (GraphPad Software, La Jolla California USA). The results are presented as averages ± SD (standard deviation) of three independent biological replicates.

In vitro activity against trypomastigotes of *T. cruzi*

$5x10^6$ parasites per well were seeded in black 96 well plates in RPMI medium with increasing concentration of compounds for 24 h. A broad range of compound concentrations was tested for each compound to estimate the IC_{50} value (0-96 µM) and then this range was narrowed according to the calculated IC_{50} to reach an accurate value; particularly, 0-48 µM for CTZ, phen, aminophen, bipy, dmb, $[Re(CO)_3(phen)(CTZ)]PF_6$, $[Re(CO)_3(aminophen)(CTZ)]PF_6$, $[Re(CO)_3(tmp)(CTZ)]PF_6$, $[Re(CO)_3(bipy)(CTZ)]PF_6$ and $[Re(CO)_3(dmb)(CTZ)]PF_6$, 0-20 µM for tmp free ligand. Viability was tested using 10 µL of alamar Blue™ (Thermo Fisher) as described above.

Cytotoxicity on VERO cells

For the cytotoxicity assay, 10000 cells per well were seeded in a 96 well plate in RPMI medium and were incubated at 37 °C in a 5 % CO_2 atmosphere. Once adhered to the plate, cells were incubated with the indicated compound concentrations for 24 h: 0-96 µM for

$[Re(CO)_3(tmp)(KTZ)]PF_6$ complex, CTZ, KTZ, phen, aminophen and tmp free ligands; 0-144 μM for bipy and dmb free ligands; 0-40 μM for $[Re(CO)_3(phen)(CTZ)]PF_6$, $[Re(CO)_3(aminophen)(CTZ)]PF_6$, $[Re(CO)_3(tmp)(CTZ)]PF_6$, $[Re(CO)_3(bipy)(CTZ)]PF_6$ and$[Re(CO)_3(dmb)(CTZ)]PF_6$. Cell viability was assessed using MTT (3-(4, 5-dimethylthiazolyl-2)-2, 5-diphenyltetrazolium bromide) assay, where MTT is reduced by metabolically active cells to generate reducing equivalents such as NADH and NADPH, resulting in the intracellular formation of a purple formazan product which can be solubilized by the addition of DMSO. Briefly, after compound incubation, 20 μL of MTT 5 mg/mL were added to each well. Plates were incubated for 4 h at 37°C in a 5 % CO_2 atmosphere. After incubation, the medium was removed and the cells were disrupted with 100 μL of DMSO. Plates were kept for 15 min with agitation and absorbance was measured at 570 nm in a Thermo Scientific Varioskan® Flash Multimode instrument. Each assay was performed three times.[59]

Confocal Raman Microscopy

Parasites were treated with compound concentrations of 1x and 10x the IC50 value for 4 and 24 hours before being deposited into a silicon substrate and dried under nitrogen flow. Untreated control parasites were also included in the analysis.

Confocal Raman Microscopy analysis was performed utilizing a WITec Confocal Raman Microscope Alpha 300 RA upgraded for Atomic Force Microscopy (AFM). In order to avoid damage to the cells an excitation laser wavelength of 532 nm was used, and the source power was adjusted. Images were obtained from scan width and scan height of 6 μm x 6 μm with grids of 35 points per line and 35 lines per image, with an adquisition time of 0.5 seconds for each spectrum.

Insight into the mechanism of action

DNA interaction studies

Electronic absorption spectrometry studies

Electronic absorption spectrometry experiments were employed to analyze the direct interaction of the complexes with calf thymus DNA (CT-DNA). DNA stock solutions were prepared by hydrating CT-DNA in Tris-HCl buffer pH 7.4 (1 mg mL^{-1}, ~2mM nuc^{-1}). The concentration of the stock solution was determined by UV spectrophotometry using the molar absorption coefficient ε (260 nm) = 6600 $M^{-1}cm^{-1}nuc^{-1}$.[62] The stock solutions of the compounds were prepared in DMSO at 1.0 mM and subsequently diluted in Tris-HCl buffer. Titration experiments were registered in the 240−400 nm range on a Thermo Scientific Evolution 60 Spectrometer using a fix concentration of compound (10 μM), while increasing the concentration of CT-DNA (0−20 μM) at room temperature. After each addition, the solutions were allowed to stand in equilibrium for 5 min before recording the spectra.[63]

Inhibition of the biosynthesis of membrane sterols

HPLC studies

The experiment was carried out on epimastigotes of *T. cruzi* (CL Brener strain) at a density of 9×10^7 parasites mL^{-1}. The compound *fac*-$[Re(CO)_3(tmp)(CTZ)](PF_6)$ was dissolved in DMSO and added at concentrations corresponding to 1× and 5× the IC_{50} value obtained from the *in vitro* assay against epimastigotes of *T. cruzi* (5.3 μM and 26.3 μM, respectively), and incubated for 4 h at 28°C. CTZ was also incubated at the same concentrations, for comparison. DMSO concentration did not exceed 0.4% v/v in the culture medium. Simultaneously, a negative control using untreated parasites and a

positive control corresponding to the drug Terbinafine were incubated. Terbinafine was incubated at a concentration equivalent to its IC_{50} on epimastigotes of *T. cruzi* (44.7 μM). After incubation, the sterols (ergosterol, lanosterol and the intermediate squalene) from the membrane of the parasites were extracted. For this task, the negative control, the positive control and the parasites treated with the compound *fac*-$[Re(CO)_3(tmp)(CTZ)](PF_6)$ and with CTZ were centrifuged at 3000 rpm for 10 min. The supernatant was discarded. The pellet was resuspended in 1 mL of phosphate buffer (0.05 M, pH = 7.4) and centrifuged again at 3000 rpm for 10 min. The supernatant was discarded, and the obtained pellet was resuspended in 1 mL of a chloroform: methanol (2:1) mixture. The obtained suspension was then kept at 4 °C for 12 h. Next, 2 mL of saturated NaCl solution was added and the mixture was extracted with 1 mL of chloroform, taking special care to avoid collecting any aqueous phase. This step was repeated twice to achieve a quantitative extraction.[64,65]

The obtained organic phase was evaporated with nitrogen and redissolved in 1 mL of acetonitrile for the subsequent determination by liquid chromatography coupled to diode array detection (HPLC-DAD). The chromatographic system used consisted of a C8 stationary phase (250 × 4.6 mm, 5 μm) and 100% acetonitrile was used as the mobile phase, at a flow rate of 0.9 mL min^{-1}. Detection was performed at 210 nm.[64,66]

Computational studies

The input geometry for the complex *fac*-$[Re(CO)_3(phen)(CTZ)]^+$ was extracted from the solved X-ray crystal structure. Starting from this information, the initial geometry for the other CTZ-containing compounds were built by modifying the NN ligand. All structures were optimized by DFT (B3LYP/LANL2DZ) as implemented in Gaussian 09.[67-69]

The solvent (water) was modeled by using the Truhlar and coworkers' SMD solvation model.[70] All optimum geometries were found to have only real vibrational frequencies. Although all possible spin multiplicities were taken into account ($2S+1$ = 1, 3, 5 or 7), the singlet electronic state resulted the most stable in each case. Therefore, it was employed during further analysis.

Molecular docking calculations were carried out to get insights into the mechanism of action of the complexes. Genetic algorithm was applied to dock the DFT-optimized substrates into the receptors using GOLD (v 4.1.2).[71]

As hosts the calf thymus DNA (CT-DNA; PDB: 453D) and the lanosterol 14-α-demethylase of *Trypanosoma cruzi* (CYP51; PDB: 2wuz) were employed.[72]

Their preparation, including the removal of water molecules and the assignment of ionization states and hydrogen coordinates, was carried out in MOE[73,74] using the following conditions: T = 37 °C, pH = 7.4 and ionic strength = 0.15 M. For the DNA molecule, the binding site was defined taking into account all the nucleotides in the CT-DNA, except from those located in the extremes of the biomolecule. In the case of the 14-alpha-demethylase, the binding site included the residues from subunit A located within a 6 Å sphere around the crystallized fluconazole. During the runs, the substrate dihedral angles were allowed to freely vary, except for those related to the metal center, while the DNA structure and the protein backbone were kept fixed. In order to allow for certain protein flexibility, various rotamers from the software library were considered for the following amino acids: TYR103, MET106, PHE110, TYR116, PHE290, THR295, LEU356, MET460 and VAL461. Each substrate was docked a total of 40 times and the docking modes that achieved the highest Chemscore fitness were retained and compared. For the most stable poses, estimated binding free energy (ΔG_{bind}), along with other energy terms (receptor-substrate hydrogen bond, lipophilic interactions, entropic loss upon

binding, clash penalty and internal ligand strain), were estimated through the ChemScore scoring function.[75,76] Other miscellaneous parameters were assigned the default values given by the GOLD program. The docking procedure was validated by performing the redocking of the crystallized fluconazole into the CYP51 (*vide infra*). The outputs were processed and rendered with Discovery Studio Visualizer software.[77]

Results and discussion

Synthesis and characterization of the complexes

The six compounds were synthesized through a stepwise procedure with good purities and acceptable yields (Fig. 2). In a first synthetic step, two carbonyl ligands of $[ReBr(CO)_5]$ were substituted by the bidentate NN ligand under reflux in toluene leading to the five *fac*-$[ReBr(CO)_3(NN)]$ precursors. In a second step, bromide was substituted by triflate using silver triflate under reflux in THF. The triflate ligand of the *fac*-$[Re(OTf)(CO)_3(NN)]$ precursors were then substituted by the azole in MeOH medium and precipitated with hexafluorophosphate to give the expected complex.

The obtained compounds are slightly soluble in organic hydrophilic solvents, like methanol, soluble in DMSO and almost insoluble in water.

Characterization of the complexes in the solid state

Initially, C, N and H microanalyses showed no adequate agreement with the proposed formula. Hardly degradable organic and organometallic compounds have traditionally given problems for the determination of elemental analyses.[78] It was detected that the Re complexes developed in this work did not fully burn in the common elemental analyzer conditions. Therefore, the classical method had to be modified by adding V_2O_5 as

catalyzer to the sample to allow complete decomposition and proper analysis, which allowed to get acceptable microanalysis results. In addition, we developed and reported a microwave plasma atomic emission spectrometry (MP-AES) method to determine Re % in order to confirm nature and purity of the compounds.[43] The analytical method was previously validated, and it proved to be an excellent alternative for Re elemental analysis, according to the obtained figures of merit.[43] Rhenium elemental analysis results fit with the proposed formula for the new Re(I) complexes.[43]

Rhenium elemental analysis results fit with the proposed formula for the new *fac*-[$Re(CO)_3(NN)(CTZ)](PF_6)$ complexes and for *fac*-[$Re(CO)_3(tmp)(KTZ)](PF_6)$.

FTIR absorption bands associated with C=N and C=C molecular vibration modes of the coordinated azole and the NN ligand were tentatively assigned. The bands are in accordance with the data previously reported in the literature.[79-83]

The IR spectra display three strong carbonyl stretching bands, ν(C≡O), in the 2035–1900 cm^{-1} region, which are characteristic of monomeric pseudo-octahedral *fac*-$\{Re(CO)_3\}^+$ complexes.[33,84] The strong stretching ν(P–F) and bending δ(F-P-F) bands of the PF_6^- counterion at around 840 and 560 cm^{-1} were also identified.[85]

Crystal structure of *fac*-[$Re(CO)_3(phen)(CTZ)](PF_6$)

An ORTEP drawing[86] of the slightly better refined [$Re(CO)_3(phen)(CTZ)$] complex in the *fac*-[$Re(CO)_3(phen)(CTZ)](PF_6$) triclinic polymorph is shown in Fig. 3 and bond distances and angles within this complex and the two independent complexes in the monoclinic crystal phase are listed in Tables S3a and S3b, respectively.

All three complexes are conformers to one another and only differ mainly in the angular conformation of CTZ ligand around the Re-N σ-bond. Therefore, we shall base our structural discussion on the triclinic complex. Rhenium(I) ion is in a slightly distorted

octahedral environment, *cis*-coordinated to three carbonyl (CO) groups [Re-C bond distances in the range from 1.900(4) to 1.924(4) Å, *cis* C-Re-C angles in the 88.3(2)-89.3(2)º interval; C-O bond lengths from 1.147(6) to 1.154(6) Å and Re-C-O angles in the 176.1(4)-178.0(3)º range]. Two other *cis*-positions are occupied by a phenanthroline molecule acting as bidentate ligand through its N-atoms [Re-N bond distances of 2.171(3) and 2.179(3) Å] and defining an equatorial coordination plane nearly containing the Re(I) ion and two of the above CO ligand groups. The six-fold coordination is completed by a 1-[(2-chlorophenyl)-diphenyl-methyl]imidazole (CTZ) molecule acting as monodentate ligand through its imidazole N-atom [d(Re-N) = 2.190(3) Å]. In the monoclinic polymorph, $[Re(CO)_3(phen)(CTZ)]$ complex conformers 1 and 2 are obtained from the triclinic complex though rotations around the Re-N bond in 10.8º and 43.7º, respectively.

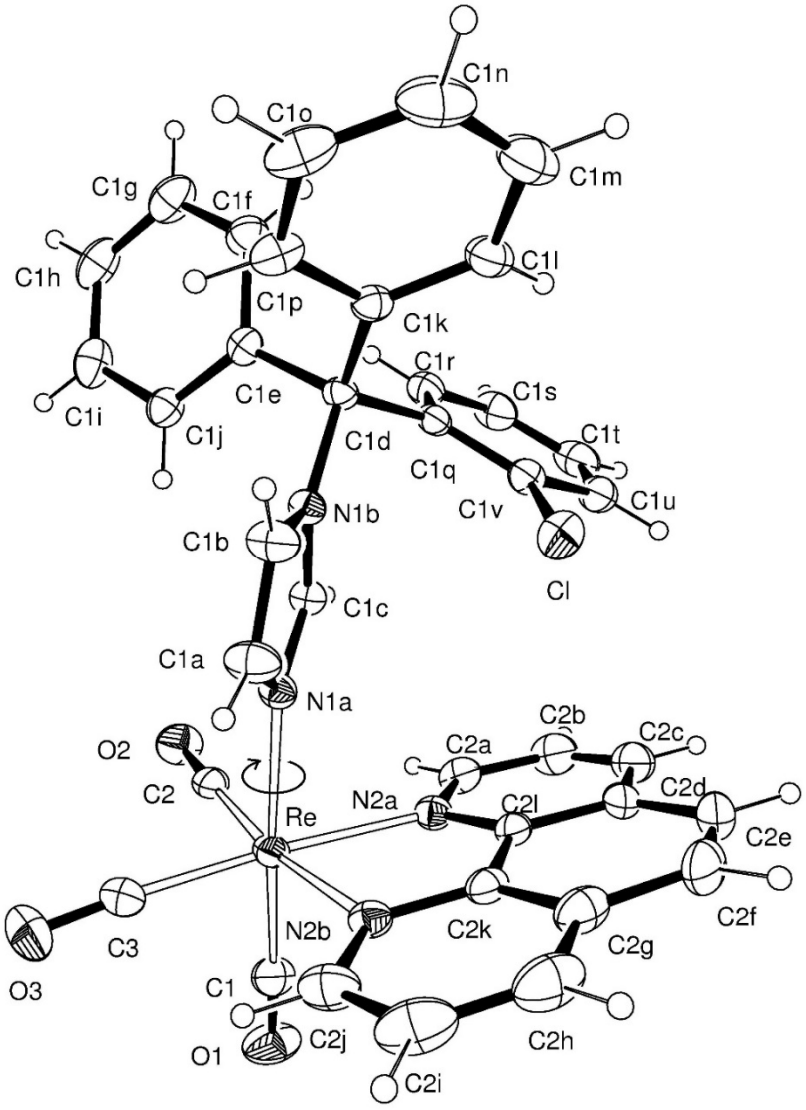

Fig. 3. View of *fac*-[Re(CO)$_3$(phen)(CTZ)] complex in the triclinic polymorph of its hexafluorophosphate salt showing the non-H atoms displacement ellipsoids at the 30% probability level. The figure shows the rotation of the organic ligand around Re-N σ-bond that brings the triclinic complex in nearly coincidence with the two conformers of the complex observed in the monoclinic polymorph.

Characterization of the complexes in solution

^{1}H-NMR results

Fig. S1 shows the numbering scheme of the ligands in all complexes. ^{1}H NMR spectra and two-dimensional COSY and HSQC NMR experiments were recorded to completely characterize the obtained complexes in DMSO-d_6 solution. All the complexes showed a pattern of signals corresponding to the protons of the azole (CTZ or KTZ) and the NN derivative (phen, dmb, bipy, aminophen or tmp) ligands. Integrations and multiplicities of the signals were in accordance with the obtained stoichiometry of the complexes (Figs. S2-S7).

In the region of 6.5 – 9.7 ppm, signals of the protons of the azoles and the NN derivatives were observed and assigned. Because of metal coordination, the signals of the protons of the azole moiety shifted, particularly the signal corresponding to H_1 and H_2, adjacent to the coordination site. In the case of the NN derivatives, 4 signals were assigned for bipy, tmp, dmb and phen, while 8 signals were assigned for aminophen. For complexes with tmp, dmb and KTZ, signals around 2.5 – 3.0 ppm corresponding to the methyl substituents were observed, as expected.

Stability in solution

During the design and development of potential metal-based drugs, the analysis and optimization of stability play a very important role, generally in the early stages of the process.[87] Metabolic stability is understood as the susceptibility of a given chemical compound to suffer biotransformation *in vivo*. In this regard, to obtain initial information of the stability of the synthesized compounds, *in vitro* tests were performed by incubating the studied compounds in different culture media used for biological assays.[50]

Monitoring was performed by HPLC-DAD technique. Chromatograms obtained at the initial time (t_1) and at the final time (t_2) were compared by evaluating both the shapes and the areas of the chromatographic peaks. Likewise, chromatograms were compared against the chromatograms of the free ligands, independently injected under the same chromatographic conditions.

Retention times were between 22 – 23 minutes for the studied Re compounds, being higher than those of the free ligands, which were in the range 14 – 21 min. So, retention time of each compound did not coincide with the retention time of the corresponding ligand. Besides, the retention times of the compounds did not vary significantly in the different assayed media. Likewise, the appearance of new signals was not observed during monitoring time. Thus, the unaltered shape of the peak over time, as well as the non-significant variation of the associated area, reflects the stability of the compounds in the studied media. In summary, the chemical stability of the *fac*-[$Re(CO)_3(NN)(CTZ)](PF_6)$ compounds in the assayed media was confirmed for a period of 5 days for DMSO and DMSO: synthetic biological medium (50:50) and for a period of 1 day for DMSO:supplemented BHI medium and DMSO:fetal bovine serum (50:50). However, for *fac*-[$Re(CO)_3(tmp)(KTZ)](PF_6)$ compound, a significant decrease of 35% in its peak area was observed in DMSO:fetal bovine serum (50:50), showing that this complex is partially decomposed in the evaluated medium during this time period. Obtained chromatograms are shown in Figs. S8 and S9.

Stability in Human plasma

As shown in Table S4, *fac*-[$Re(CO)_3(NN)(CTZ)](PF_6)$ compounds were stable in human plasma for a period of 24 h. This can be assured from the practically constant ratio of the analyzed compound with respect to the internal standard ($A_{Compound}/A_{Caffein}$, where A is the area under the peak) and the non-appearance of new chromatographic peaks over time. This ratio was used for stability monitoring after having been normalized to 100 %. This strategy poses the advantage that the analytical recovery rate of the compound does not affect the experiment results. On the other hand, *fac*-[$Re(CO)_3(tmp)(KTZ)](PF_6)$ started to decompose in human plasma after being incubated for 1 h. As shown in Table S4, after

1 h the $A_{Compound}/A_{Caffein}$ dropped to half its value, meaning that the complex concentration dropped to 50% its initial value, while a second signal (2nd peak, as mentioned in Table S4) appeared, as shown in Fig. 4. This splitting of the peak would be associated with the partial decomposition of the compound studied.

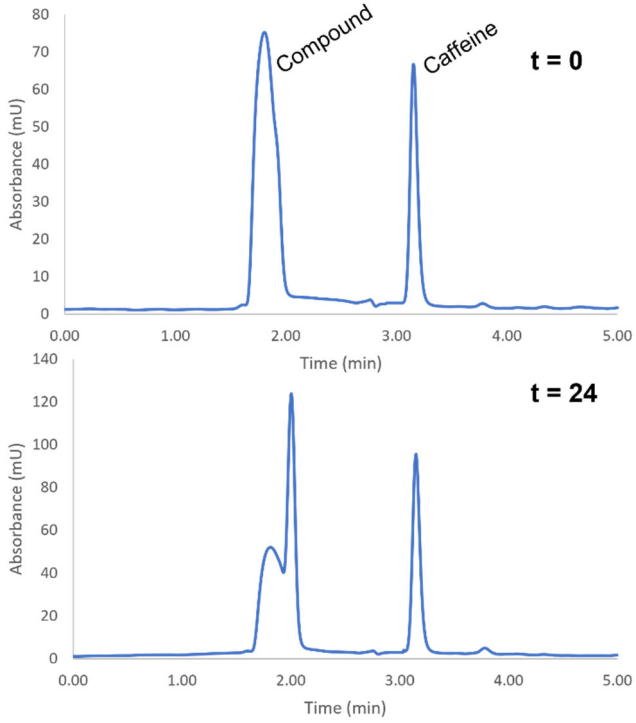

Fig. 4. Chromatograms obtained for *fac*-[Re(CO)$_3$(tmp)(KTZ)](PF$_6$) compound at t=0 and t=24 h.

Lipophilicity

Lipophilicity is an important property of bioactive molecules in relation to their biological activity that can determine the behavior of a potential drug in a given biological medium. It is related to the distribution of a potential drug through the blood-brain barrier and the intestinal absorption and is determinant for the ability to penetrate biological membranes in general.[53,88,89] Therefore, the study of the lipophilicity is of great importance from the pharmacokinetic point of view, especially influencing the absorption, distribution,

excretion, and toxicity of potential drugs.[90,91] All this makes it an important property when designing new drugs. It is also important to determine if there is a correlation between the lipophilicity of a given compound and its biological activity.

In this regard, RP-HPLC technique has been used as a tool for the evaluation of lipophilicity for a long time since most of the hydrophobic forces dominate the retention process.[53] It is very useful for the study of complex systems, in which the separation of the studied compounds is made difficult by batch thin-layer chromatography methods.

Different chromatographic conditions were tested in order to separate the six compounds of interest in a single isocratic run. Once the chromatographic conditions were optimized, the chromatogram observed in Fig. 5 was obtained, with the retention times (t_R) of the complexes being 14.82 min (Re-phen-CTZ), 18.09 min (Re-dmb-CTZ), 18.92 min (Re-bipy-CTZ), 25.41 min (Re-aminophen-CTZ), 29.28 min (Re-tmp-CTZ), and 32.09 min (Re-tmp-KTZ), respectively. Hold-up time was 3.48 min (tartrazine).

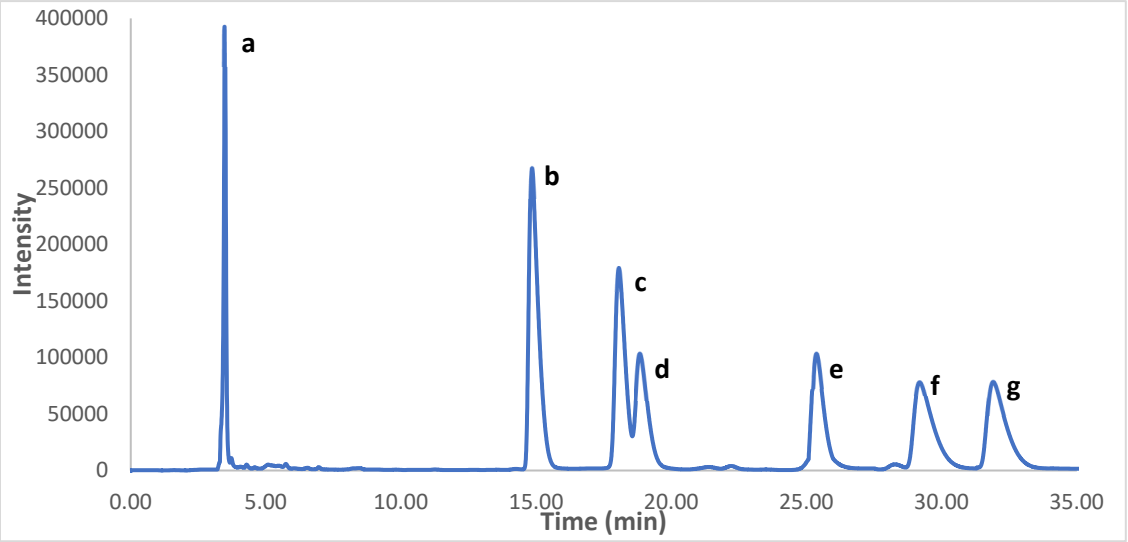

Fig. 5. Chromatogram obtained for the mixture of the six Re-Azole-NN compounds and tartrazine: (a) tartrazine, (b) Re-phen-CTZ, (c) Re-dmb-CTZ, (d) Re-bipy-CTZ, (e) Re-aminophen-CTZ, (f) Re-tmp-CTZ, (g) Re-tmp-KTZ.

The chromatographic parameters t_0 and t_R were used to calculate R_F parameter according to reports from Bate-Smith & Westall,[92]

with t_C being the total time of the run of 35 min. Likewise, the R_M parameter was calculated for each compound. The equations are described below[92]:

$$R_F = \frac{t_R - t_0}{t_C} \qquad R_M = log_{10}(\frac{1}{R_F} - 1)$$

Since R_M values vary directly with the partition coefficient and also, in many cases, change by equal increments with each successive addition of a particular substituent group, they are more useful than the corresponding R_F values. A particularly useful property of R_M parameter, when compared to R_F parameter, is that the former is a simple function of the temperature and the relative volumes of the solvent phases.[92] Besides, several series of potential chemotherapeutic agents can be compared in the same chromatographic system using this strategy. A higher R_M value is associated with a higher degree of polar substitution. On the other hand, a negative R_M value is obtained when the term $[(1/R_F) - 1]$ is less than 1, which is achieved when a high enough R_F is observed for the analyzed compound, which is associated with a higher degree of nonpolar substitution and thus a higher lipophilicity.[92]

Table 1. Chromatographic parameters t_R, R_F and R_M obtained for each compound.

Compound	**t_R (min)**	**R_F**	**R_M**
Tartrazine	3.48	R_F	R_M
fac-[Re(CO)$_3$(phen)(CTZ)](PF$_6$)	14.82	0.32	0.32
fac-[Re(CO)$_3$(dmb)(CTZ)](PF$_6$)	18.09	0.42	0.14
fac-[Re(CO)$_3$(bipy)(CTZ)](PF$_6$)	18.92	0.44	0.10

fac-[Re(CO)$_3$(aminophen)(CTZ)](PF$_6$)	25.41	0.63	-0.22
fac-[Re(CO)$_3$(tmp)(CTZ)](PF$_6$)	29.28	0.73	-0.45
fac-[Re(CO)$_3$(tmp)(KTZ)](PF$_6$)	32.09	0.82	-0.65

The classical *shake flask* method led to similar results (Table 2).

Table 2. Distribution coefficients of *fac*-[Re(CO)$_3$(NN)(*N*-azole)](PF$_6$) complexes between octanol and aqueous phosphate

Compound	**LogP**
fac-[Re(CO)$_3$(phen)(CTZ)](PF$_6$)	2.85
fac-[Re(CO)$_3$(dmb)(CTZ)](PF$_6$)	3.18
fac-[Re(CO)$_3$(bipy)(CTZ)](PF$_6$)	4.00
fac-[Re(CO)$_3$(aminophen)(CTZ)](PF$_6$)	ND*
fac-[Re(CO)$_3$(tmp)(CTZ)](PF$_6$)	4.26
fac-[Re(CO)$_3$(tmp)(KTZ)](PF$_6$)	6.69

*The lipophilicity of *fac*-[Re(CO)$_3$(aminophen)(CTZ)](PF6) could not be obtained by this method since it decomposes during the determination.

According to the obtained results (Tables 1 and 2), it can be concluded that lipophilicity of the compounds, presented in increasing order, is as follows: *fac*-[Re(CO)$_3$(phen)(CTZ)](PF$_6$) < *fac*-[Re(CO)$_3$(dmb)(CTZ)](PF$_6$) < *fac*-[Re(CO)$_3$(bipy)(CTZ)](PF$_6$) < *fac*-[Re(CO)$_3$(aminophen)(CTZ)](PF$_6$) < *fac*-[Re(CO)$_3$(tmp)(CTZ)](PF$_6$) < *fac*-[Re(CO)$_3$(tmp)(KTZ)](PF$_6$).

After comparing these results to those obtained from biological assays, it can be concluded that the compound presenting the highest lipophilicity, *fac*-[$Re(CO)_3(tmp)(CTZ)](PF_6)$, is clearly the most active against *T. cruzi*. Nevertheless, the lipophilicity/activity relationship is not strictly adhered to for the other compounds.

Biological studies

Anti-*Trypanosoma cruzi in vitro* activity, cytotoxicity on VERO cells and selectivity towards the parasite

To determine the antiproliferative properties of these Re(I) tricarbonyls, the IC_{50} values of each compound and the respective free ligands were determined through viability assays after parasite incubation with different compound concentrations. As shown in Table 3, the complexation of CTZ to $\{Re^{I}(CO)_3(NN)\}$ led to a decrease in the IC_{50} value of one order of magnitud comparing with the CTZ alone, which is interpreted as an improvement in the antiparasitic activity of the compounds. This effect was observed in both forms of the parasite, epimastigotes and trypomastigotes. In epimastigotes, the determined IC_{50} values are in the same range as that calculated for the reference drug Nifurtimox. However, in infective trypomastigotes the IC_{50} values of the compounds reach values of one order of magnitude lower than the reference drug. On the other hand, the selectivity towards the parasite did not improve through the generation of the *fac*-$[Re(CO)_3(NN)(CTZ)](PF_6)$ compounds in respect to free CTZ.

As stated in the Introduction section, the free NN ligands showed activity on *T. cruzi* trypomastigotes and epimastigotes with IC_{50} values in the micromolar range. With the exemption of the aminophen complex, the Re compounds showed increased activity, in respect to free NN ligands, on trypomastigotes, which is the relevant infective form of the parasite. Nevertheless, the new compounds showed higher cytotoxicity on VERO cells than the free NN ligands which

led to lower selectivity index values. The antiparasitic activiy of $[Re(CO)_3(tmp)(KTZ)]PF_6$ could not be properly determined due to its low solubility. Further modification of its structure is planned to achieve a solubility improvement.

Table 3. *In vitro* activity on *T. cruzi*, cytotoxicity on mammalian cells (VERO cells) and selectivity towards the parasites (SI values).

Compound	**IC_{50} VERO ± SD (μM)**	**IC_{50} *T. cruzi epimastigotes* ± SD (μM)**	**SI epimastigotes**	**IC_{50} *T. cruzi trypomastigotes* ± SD (μM)**	**SI trypomastigotes**
CTZ	37.1 ± 7.6	22.2 ± 0.5	1.7	10.2 ± 0.5	3.6
KTZ	>96	ND		89.0 ± 19.2	>1.0
phen	50.2 ± 18.7	10.2 ± 0.3	4.9	4.04 ± 0.26	12.4
aminophen	29.9 ± 4.3	9.37 ± 1.02	3.2	1.81 ± 0.55	16.5
tmp	51.9 ± 10.2	3.43 ± 0.85	15.1	6.10 ± 2.77	8.5
bipy	81.3 ± 14.0	12.5 ± 0.8	6.5	9.66 ± 0.23	8.4
dmb	95.2 ± 17.0	10.6 ± 2.4	9.0	26.2 ± 8.8	3.7
$[Re(CO)_3(phen)(CTZ)]PF_6$	3.20 ± 0.24	9.42 ± 1.53	0.34	1.28 ± 0.12	2.5
$[Re(CO)_3(aminophen)(CTZ)]PF_6$	12.8 ± 2.2	8.43 ± 2.20	1.5	2.79 ± 0.57	4.2
$[Re(CO)_3(tmp)(CTZ)]PF_6$	5.10 ± 1.60	3.48 ± 0.98	1.5	0.61 ± 0.18	8.4

$[Re(CO)_3(bipy)(CTZ)]PF_6$	6.50 ± 1.10	7.53 ± 2.68	0.89	1.11 ± 0.10	5.8
$[Re(CO)_3(dmb)(CTZ)]PF_6$	14.0 ± 4.3	8.48 ± 1.46	1.6	2.26 ± 0.11	6.2
$[Re(CO)_3(tmp)(KTZ)]PF_6$	>96.0	ND	ND	>96.0	ND
Nifurtimox	998 ± 91	7.10 ± 2.20	140	20.1 ± 2.9	49.6

SI: Selectivity index: IC_{50} mammalian cells /IC_{50} *T. cruzi*

ND: not determined.

Confocal Raman Microscopy

In previous studies by microwave plasma atomic emission spectrometry (MP-AES), $[Re(CO)_3(tmp)(CTZ)]PF_6$ showed a preferential association to the parasite soluble proteins fraction and a low association to DNA and RNA fractions, which suggested to discard these biomolecules as main targets.[43]

In order to deepen in the localization of the uptaken compound in the whole parasite, confocal Raman microscopy was performed. According to literature, signals in the range of ~1650 cm^{-1} correspond to Amide I C=O stretching mode (proteins and DNA, Fig. 6 red region), signals in the range of 1425/1475 cm^{-1} correspond to CH_2/CH_3 anti-symmetric methyl/methylene deformations (lipids, Fig. 6 blue region) and signals in the range of 1570/1580 cm^{-1} correspond to C=C stretching modes in purine bases (DNA/RNA, Fig. 7 red region).[93-95] Additionally, the signal at 1594 cm^{-1} observed in Fig. 6 (green region) could be attributed to DNA in higher concentration. On this basis, the red and green label correspond to mitochondrial and nuclear DNA and the blue label to lipids from the membrane.

The main bands of the Re(I) tricarbonyl compound show a strong overlap with signals coming from lipids, proteins and DNA and, due to its low concentration in the parasite, signals associated to $\nu(CO)$ stretching modes are not so pronounced in Raman spectroscopy for being detected in our experiments. Therefore, we focused on the main changes occurring in treated parasites relative to untreated control parasites.

It is worth noting that previous determinations by MP-AES of rhenium association to parasite DNA fraction were performed after biomolecule extraction and purification processes.[43] Consequently, the amount of metal determined by this technique corresponds only to that strongly bound to the biomolecule.

Notwithstanding, the overlap found by confocal Raman gave us a clue to the actual location inside the parasite. Comparing confocal Raman images obtained for 1x IC_{50} treated parasites for 4 h, and 24 h with untreated control parasites (Fig. 6) it can be observed that the signals associated to DNA suffer important changes in their localization along the parasite, indicating a possible weak interaction with the compound as shown in the following section.

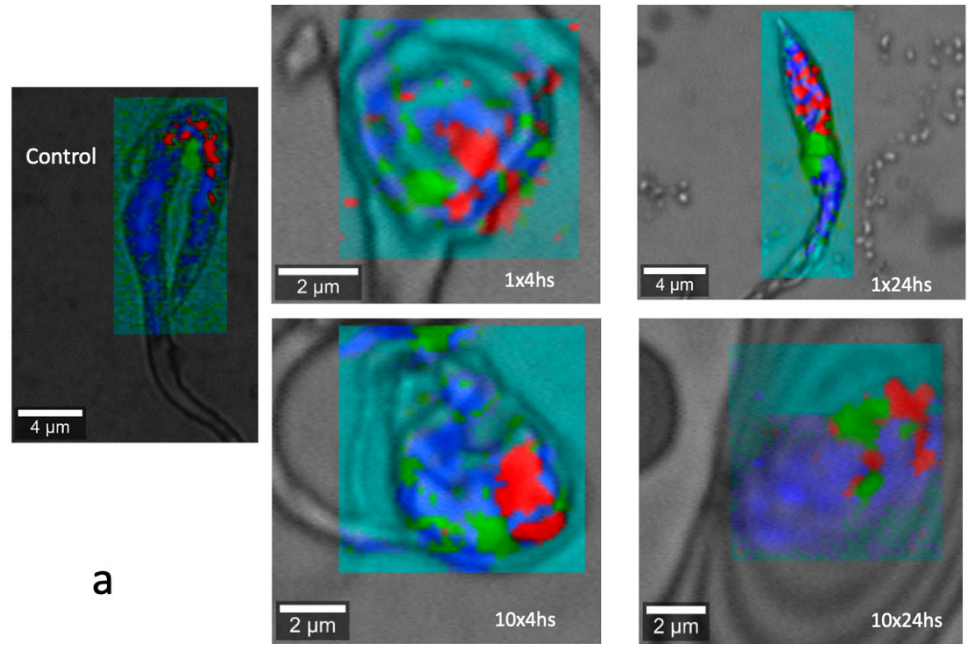

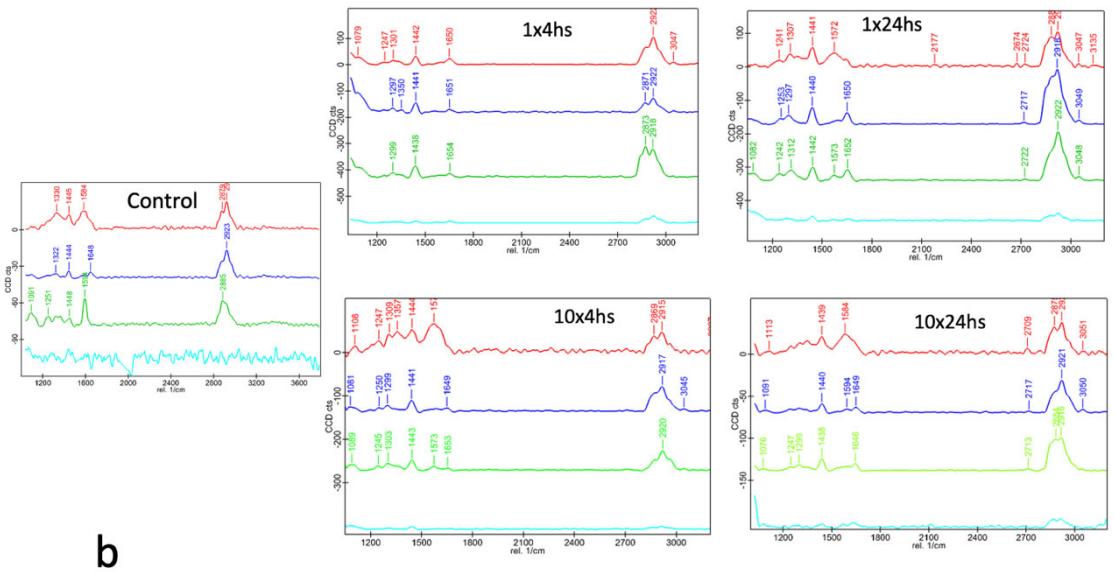

Fig. 6 a) Overlay between optical and confocal Raman images as obtained from selected principal components analysis for samples: control, 1x 4 h, 1x 24 h, 10x 4h and 10x 24 h. **b)** Average Raman spectra for each component, as corresponding with confocal Raman images presented in (a).

Insights into the mechanism of action

DNA interaction studies

DNA binding studies by electronic absorption spectrometry

The direct binding of the compounds with CT-DNA was evaluated by monitoring the changes in the electronic spectra while increasing concentration of CT-DNA. Upon addition of DNA, a slight hyperchromism was noticed in the UV region (270–320 nm) (Fig. S10).

According to the literature, a hyperchromic effect arises mainly due to the presence of charged cations which interact with DNA via electrostatic attraction to the phosphate groups of DNA backbone thereby causing a contraction and overall damage to the secondary structure of DNA. The effect may also be attributed to external contact (electrostatic binding) or to partial uncoiling of the helix structure of DNA, exposing more bases of the DNA. On the other hand, compounds binding to DNA through intercalation usually show hypochromic and bathochromic effects when the concentration of DNA is increased due to the combination of π electrons of the compound and π electrons of DNA bases.[96]

Regarding DNA intercalation capabilities, these results match with results of competitive studies on the CT-DNA-Ethidium bromide adduct, performed with the most active compound Re-CTZ-tmp by quenching of fluorescence measurements.[97] As shown in Fig. S11, negligible intercalation effect in CT-DNA was observed. In conclusion, the new complexes do not show

strong intercalating interaction with this biomolecule but interact through other mechanism, probably involving electrostatic interactions.

Molecular docking on CT-DNA

With the aim of elucidating the structural aspects behind the binding of the compounds to CT-DNA, molecular docking calculations were performed. Since no intercalation was observed experimentally, the receptor was kept fixed, giving certain flexibility to the complexes (see the experimental section for further details). Each substrate was docked 40 times, and the results are depicted in Fig. S12. In general terms, the docking poses display a high level of structural variability, with RMSD values in the range 18 - 29 Å. This suggests an interaction where the complexes do not have a significantly preferred anchoring pose, even though the binding site is always located in the DNA major groove.

Taking into account the best ranking pose in each case, the five $[Re(CO)_3(NN)(CTZ)]^+$ complexes bind to the CT-DNA with similar affinity, with estimated ΔG_{bind} values ranging from -17.5 to -18.9 kJ/mol (Table S5). This is the reflection of the fact that the binding schemes share some similar features, even though there are some differences worth pointing out. Indeed, according to the Chemscore energy terms, while the Re-aminophen-CTZ complex displays the strongest H-bonds with the receptor, the rest of the complexes establish lipophilic interactions of higher intensity. To reveal the specific structural details of the binding modes, Figs. 7 and S13 show the best ranking poses docked into the CT-DNA receptor. When NN is phen, bipy, dmb, or tmp, the complexes fit the major groove of the DNA by establishing conventional and C-H H-bonds with cytosine and the phosphate-sugar skeleton using the carbonyl ligands (Figs. 7a, 7c and S13). The pose is further stabilized by π-sigma interactions established between the CTZ phenyl rings and thymine. In the case of $[Re(CO)_3(aminophen)(CTZ)]^+$, the binding mode is slightly different. The amino group of the NN ligand establishes a strong N-H···O H-bond

with the phosphate skeleton, forcing the complex to rotate within the major groove (Figs. 7b and 7d). The carbonyl ligands are directed to the nucleotide basis, stabilized by the formation of H-bonds with adenine and the phosphate-sugar backbone. The pose is finally secured by the establishment of a CTZ-thymine π-sigma interaction.

The structural information on the complexes' binding modes gives further evidence to rationalize the observed hyperchromism during the DNA binding studies. It is feasible that the cation complexes approach the DNA molecule, fitting into de major grove by setting up H-bonds and π-sigma interactions with the nucleotide basis and the phosphate-sugar backbone, which leads to a concomitant distortion to the DNA secondary structure.

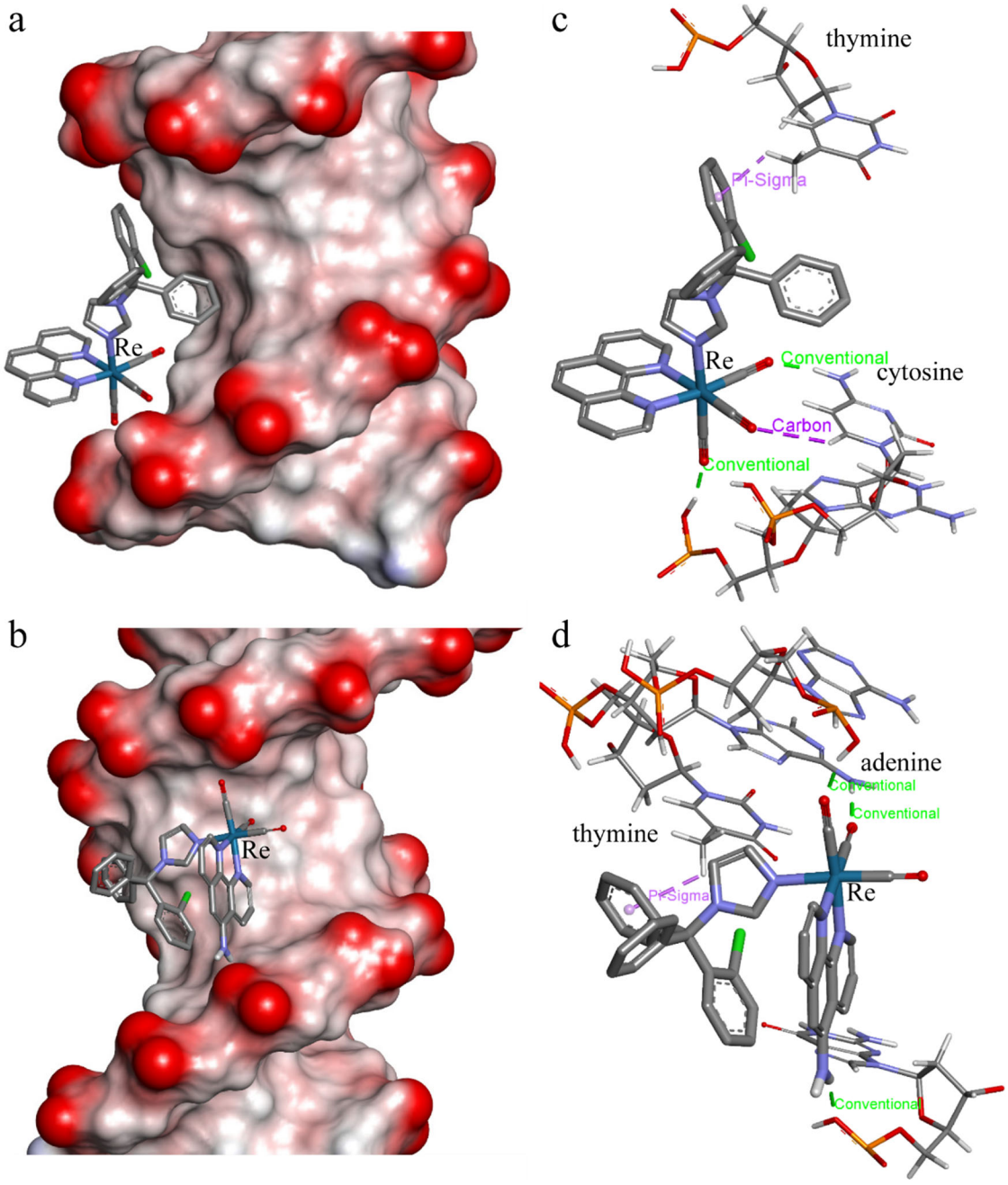

Fig. 7. Model of *fac*-[Re(CO)$_3$(phen)(CTZ)]$^+$ (a) and *fac*-[Re(CO)$_3$(aminophen)(CTZ)]$^+$ (b) docked into the major groove of CT-DNA. In both cases, the solvent-accessible surface is depicted for the receptor, with the interpolated atomic charges mapped on it. In (c) and (d), the intermolecular interactions between the substrate and the CT-DNA are shown for (a) and (b), respectively. Pi-sigma = C-H-π interaction; conventional = conventional H-bond; Carbon = C-H H-bond. Atom color code: C (grey), N (blue), O (red), Cl (green), H (white).

Inhibition of the biosynthesis of membrane sterols

Ergosterol biosynthesis in *Trypanosoma cruzi* has been validated as a chemotherapeutic target in several steps of its route, including inhibition of the enzymes squalene-2,3-epoxidase (catalyzes the conversion of squalene to squalene-2,3-epoxide), lanosterol synthase (catalyzes the conversion of squalene-2,3-epoxide to lanosterol), lanosterol 14-α-demethylase (catalyzes the conversion of lanosterol to 4,4-dimethyl-5α-cholesta-8,14,24,trien-3-β-ol), among others.[64,65]

In this regard, ergosterol, lanosterol and squalene levels in control parasites and parasites incubated with the most active compound *fac*-[$Re(CO)_3$(tmp)(CTZ)](PF_6) and with CTZ were evaluated to establish potential targets along the biosynthetic route.

Terbinafine inhibits squalene-2,3-epoxidase but also lanosterol 14-α-demethylase, leading to accumulation of squalene and lanosterol.[65]

As can be observed in Table 4, parasites treated with the compound [*fac*-$Re(CO)_3$(tmp)(CTZ)](PF_6) were also able to accumulate squalene and lanosterol with the concomitant decrease in ergosterol levels. The accumulation capacity of squalene and lanosterol, when the parasite was incubated at a concentration of 5 × IC_{50}, was slightly lower than that observed for the drug Terbinafine. In all cases, ergosterol concentration was lower than the values of the untreated parasites, being the depletion promoted by Terbinafine the highest. This fact could indicate some differences in the mechanism of action between the studied compound and Terbinafine. The fact that lanosterol is accumulated in greater proportion could be an indicator that the compound *fac*-[$Re(CO)_3$(tmp)(CTZ)](PF_6) would mainly possess inhibitory capacity at the level of the enzyme lanosterol 14-α-demethylase, as previously reported for Clotrimazole.[98]

Inhibition of this cytochrome P-450-dependent enzyme, which converts lanosterol to ergosterol, would result in an unstable cell wall in the parasite and cause membrane leakage.[99]

Besides, the fact that ergosterol depletion is higher for the studied complex, when compared to Clotrimazole, indicates that the complex poses a higher inhibitory activity than the corresponding ligand, as shown in Table 5.

Table 4. Squalene, lanosterol and ergosterol quantification in epimastigotes of *Trypanosoma cruzi* after 4 h incubation.

Sterol	**NC**	**Compound 1x**			**Compound 5x**			**Terbinafine**		
	C (μmol L^{-1})	C (μmol L^{-1})	A (%)	D (%)	C (μmol L^{-1})	A (%)	D (%)	C (μmol L^{-1})	A (%)	D (%)
Ergosterol	10.92	8.42	---	22.8	7.87	---	27.9	6.61	---	39.6
Lanosterol	6.07	7.10	16.9	---	7.99	31.7	---	8.62	42.2	---
Squalene	11.35	12.00	5.8	---	12.29	8.4	---	12.83	13.0	---

NC: Negative control; A(%): Accumulation percentage; D(%): Depletion percentage.

Table 5. Squalene, lanosterol and ergosterol quantification in epimastigotes of *Trypanosoma cruzi* after 4 h incubation with CTZ.

Sterol	**Clotrimazole 1x**			**Clotrimazole 5x**		
	C (μmol L^{-1})	A (%)	D (%)	C (μmol L^{-1})	A (%)	D (%)
Ergosterol	8.82	---	19.2	8.19	---	24.9
Lanosterol	6.98	15.0	---	7.82	28.9	---
Squalene	11.71	3.2	---	12.10	6.7	---

A(%): Accumulation percentage; D(%): Depletion percentage.

Interaction with lanosterol 14-α-demethylase: a molecular docking picture

According to the experimental evidence, the complex $[Re(CO)_3(tmp)(CTZ)]^+$ displays inhibitory capacity towards the enzyme lanosterol 14-α-demethylase of *Trypanosoma cruzi* (CYP51). While we demonstrated that the compound is stable in biological medium, it is still possible that CTZ is released, allowing for a binding to CYP51. Alternatively, the whole compound could bind to the enzyme. To furnish a picture of the mechanism of action, we proceeded to perform molecular docking calculations of this complex and CTZ, employing CYP51 as a receptor (see the experimental section for further details).

Figs. 8a and 8b depict the crystal structure of the enzyme in complex with fluconazole. It is composed by two subunits (A and B), each one bearing a hydrophobic tunnel leading to a heme-containing active site.[100]

The fluconazole molecule is stabilized inside the active site through a coordinative bond between the iron cation and the aromatic nitrogen atom of a triazole ring (Fig. S14a). The substrate conformation is also secured by H-bonds established with THR295 and TYR103, in conjunction with multiple π-alkyl interactions with ALA291, VAL461, LEU356, MET460, MET106 and the heme group. Using this information, the molecular docking protocol was validated by a redocking of the fluconazole inhibitor. The results, depicted in Fig. S14b, reveal an excellent performance of the computational model, with an RMSD between the best ranking pose and the crystallized conformation as low as 1.45 Å.

Concerning the docking of $[Re(CO)_3(tmp)(CTZ)]^+$ complex inside CYP51, the computational results show that the best ranking pose (Figs. 8c and 8d) is located within the major cluster of solutions, comprised of 9 conformations under a RMSD of 2.96 Å. The substrate is anchored into the active site through a high number of hydrophobic interactions, including π-anion (GLU205), π-sigma (heme group, LEU356), π-π (TYR103, PHE290), π-alkyl (LEU356, VAL102, MET360, MET460, VAL461, PHE290, ALA291), alkyl (heme group, MET106,

ALA287, MET460, LEU208, VAL461, ALA291, MET360, VAL213), and π-sulfur (MET460). All those connections force the complex to direct the Rhenium coordination sphere towards the active site and near the heme group, letting the CTZ fragment to face the hydrophobic tunnel.

In the case of CTZ, the docking model shows very low structural variability. In fact, the main cluster of solutions, including the best 13 conformations, contains 22 poses within a RMSD = 1.0 Å. The best ranking pose (Figs. 8e and 8f) suggests that the binding mode is similar to that found for fluconazole. In detail, the CTZ molecule is bound to the heme group through a coordinative bond with the imidazole ring. The specific orientation inside the active site is fixed by a plethora of interactions, mostly hydrophobic: carbon hydrogen bond (ALA291), π-donor hydrogen bond (TYR103), π-anion (heme group), π-sigma (heme group, LEU356), π-π (heme group, PHE110), π-alkyl (heme group, LEU356, ALA291, PHE290), and π-sulfur (MET106). Globally, these lipophilic interactions are weaker than those found for $[Re(CO)_3(tmp)(CTZ)]^+$, giving rise to a decrease of 21.4 kJ/mol in the estimated ΔG_{bind} from CTZ to the corresponding Re(I) complex (Table S5). The stronger affinity for the receptor exhibited by $[Re(CO)_3(tmp)(CTZ)]^+$ gives a feasible explanation for its higher inhibitory capacity in comparison with CTZ.

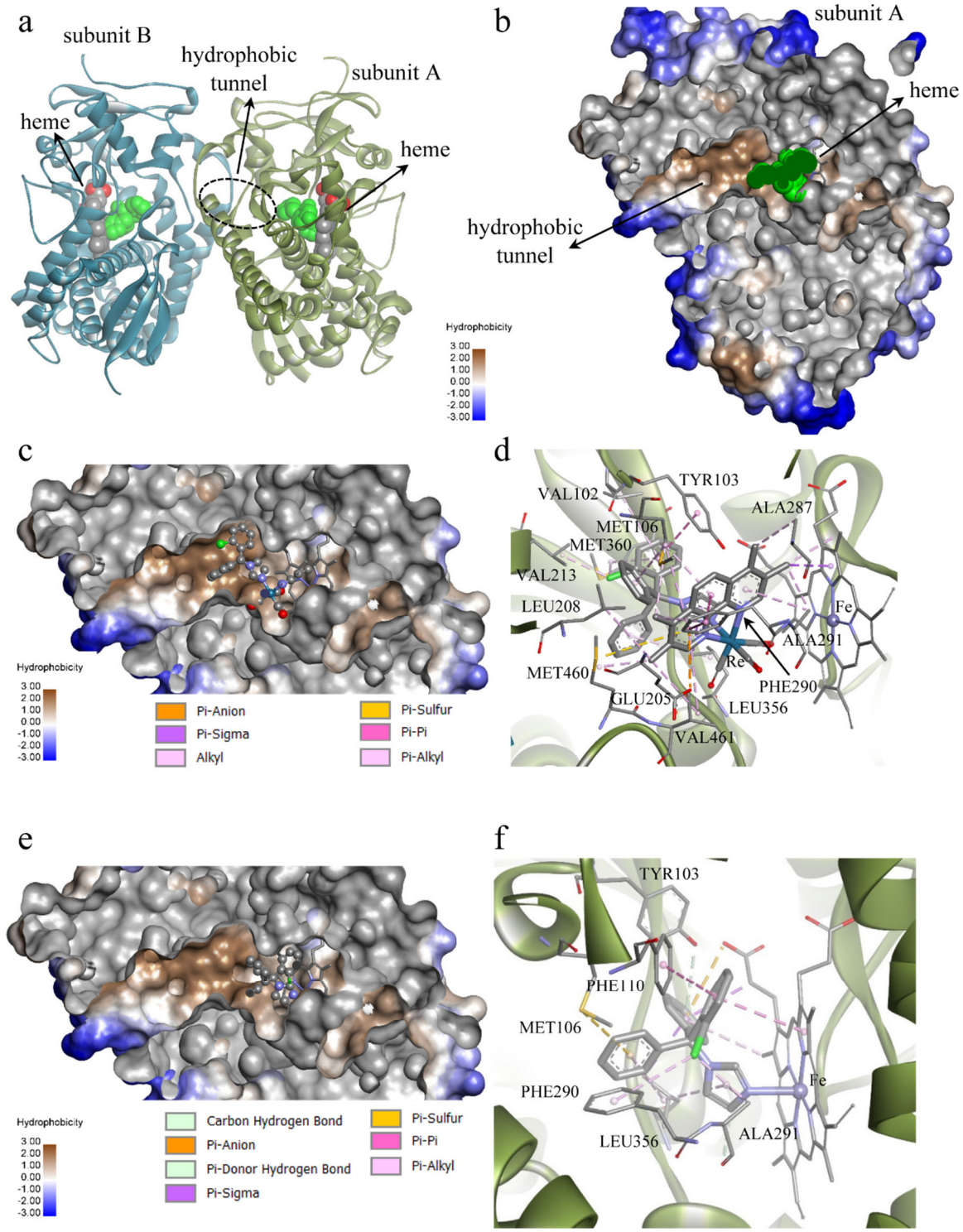

Fig. 8. a) Crystal structure of lanosterol 14-α-demethylase of *Trypanosoma cruzi* (CYP51) in complex with fluconazole. The heme group and crystallized fluconazole (green) are represented as CPK. b) Hydrophobicity is mapped onto a Connolly solvent-accessible surface

of the subunit A, applying a clipping plane to reveal the hydrophobic tunnel that leads to the active site. In c) and e), the best ranking pose are shown for $[Re(CO)_3(tmp)(CTZ)]^+$ and CTZ, respectively. The substrate-receptor intermolecular interactions are represented as colored dashed lines in d) and f), respectively. Atom color code: C (grey), N (blue), O (red), Cl (green), H (white).

Conclusions

Searching for new prospective drugs against *Trypanosoma cruzi*, the causative agent of Chagas disease, six heteroleptic multifunctional Re(I) tricarbonyls including NN polypyridyl phenanthroline derivatives and Clotrimazole or Ketoconazole as bioactive ligands were synthesized and fully characterized in solid state and in solution. The CTZ compounds showed high activity against infective trypomastigote form of the parasite with IC_{50} values in the low micromolar range and moderate to good selectivity index values tested using VERO cells as mammalian cell model. The inclusion of the two bioactive ligands in a single moiety led to compounds that are mostly more active than the free ligands. This demonstrates that the assembly rationale applied to design the Re(I) compounds was successful. The compounds were stable in different biologically relevant media, particularly for at least 24 h in DMSO:supplemented BHI medium and in human plasma. The compounds were more lipophilic than the free bioactive ligands but no correlation between antitrypanosomal activity and lipophilicity was observed. In order to assess the localization of the compounds in the whole parasite, confocal Raman microscopy was performed. The low intensity of the tricarbonyls stretching did not allow to assure the localization of the complexes in the parasites. In order to unravel the mechanism of action of the compounds two potential targets were experimentally and theoretically studied: DNA and one of the enzymes involved in the

ergosterol biosynthetic pathway, CYP51 (lanosterol 14-α-demethylase). As hypothesized, the multifunctional compounds share *in vitro* a similar mode of action as that disclosed for the single bioactive moieties included in the new chemical entities. The whole set of results show the potentiality of these Re(I) tricarbonyls as promising candidates for further antitrypanosomal drug development.

Conflicts of interest

There are no conflicts of interest to declare.

Acknowledgements

M.S. acknowledges the support of the Agencia Nacional de Investigación e Innovación (ANII, Uruguay) through the Master grant POS_FCE_2020_1_1009195. This work was supported by Agencia Nacional de Investigación e Innovación (ANII, Uruguay) through the project grant FCE-1_2019_1_155971. Additionally, it was supported by ECOS-Sud action U20E02, CONICET (PIP 0651) and UNLP (Grant to Project 11/X857) of Argentina. GAE and OEP are Research Fellows of CONICET, Argentina. This work was financially supported by an ERC Consolidator Grant PhotoMedMet to G.G. (GA 681679) and has received support under the program *Investissements d'Avenir* launched by the French Government and implemented by the ANR with the reference ANR-10-IDEX-0001-02 PSL (G.G.).

Author contributions

Conceptualization: GS, MS, RF, LPD, IM, DG.

Validation: IM, DG.

Formal analysis: MS, GS, LPD, IM.

Investigation: MS, GS, FC, NP, NV, RF, LPD, IM.

X Ray diffraction study: GAE, OEP

Resources: GG, LPD, IM, DG.

Writing original draft: IM, DG.

Writing - Review & Editing: MS, GS, RF, GG, LPD, IM, DG.

Visualization: IM, DG.

Supervision: IM, DG.

Project administration: IM, DG.

References

1. C.J. Perez, A.J. Lymbery, R.C.A. Thompson, *Trends Parasitol.* 2015, **31**, 595-603.
2. S.S. Santos, R.V. de Araujo, J. Giarolla, O.E. Seoud, E.I. Ferreira, *Int. J. Antimicrob. Agents* 2020, **55**, 105906. doi:10.1016/j.ijantimicag.2020.105906.
3. World Health Organization. Chagas disease (American trypanosomiasis). https://www.who.int/health-topics/chagas-disease#tab=tab_1. visited 2022.
4. R. Paucar, E. Moreno-Viguri, S. Perez-Silanes, *Curr. Med. Chem.* 2016, **23**, 3154-3170.
5. World Health Organization (2012). Why are some tropical diseases called 'neglected'? https://www.who.int/features/qa/58/en/. visited 2022.
6. World Health Organization Neglected tropical diseases. https://www.who.int/news-room/q-a-detail/neglected-tropical-diseases. visited 2022.
7. A.F. Francisco, S. Jayawardhana, F. Olmo, M.D. Lewis, S.R. Wilkinson, M.C. Taylor, J.M. Kelly, *Molecules* 2020*,* **25**, 1-14.

8. C.B. Scarim, D.H. Jornada, R.C. Chelucci, L. de Almeida, J.L. Dos Santos, M.C. Chung, *Eur. J. Med. Chem*. 2018, **155**, 824-838.
9. E. Chatelain, J.R. Ioset, *Expert Opin. Drug. Discov.* 2018, **13**, 141-153.
10. O.T. Kayode, C.K. Lele, A.A.A. Kayode, *Glob. J. Infect. Dis. Clin. Res*. 2020, **6**, 37-41.
11. D. Gambino, L. Otero, *Front. Chem.* 2022, **9**, 816266. doi: 10.3389/fchem.2021.816266.
12. D. Gambino, L. Otero, *Met. Ions Life Sci.* 2019, **19**, 331–357.
13. D. Gambino, L. Otero, *Inorganica Chim. Acta* 2018, **472**, 58-75.
14. D. Gambino, L. Otero, *Inorganica Chim. Acta* 2012, **393**, 103–114.
15. D. Gambino, *Coord. Chem. Rev.* 2011, **255**, 2193-2203.
16. J. C. Pessoa, S. Etcheverry, D. Gambino, *Coord. Chem. Rev.* 2015, **301**, 24-48.
17. R.A. Sánchez-Delgado, A. Anzellotti, *Mini-Rev. Med. Chem.* 2004, **4**, 159 – 165.
18. R.A. Sánchez-Delgado, A. Anzellotti, L. Suárez, in: H. Sigel, A. Sigel (Eds.), Metal Ions in Biological Systems 41: Metal Ions and Their Complexes in Medication, Marcel Dekker, New York, 2004, p. 379.
19. Y. C. Ong, S. Roy, P.C. Andrews, G. Gasser, *Chem. Rev.* 2019, **119**, 730–796.
20. R.W. Brown, C.J.T. Hyland, *MedChemComm* 2015, **6**, 1230–1243.
21. M. Navarro, *Coord. Chem. Rev.* 2009, **253**, 1619-1626.
22. M. Navarro, R.M.S. Justo, G. Y. Sánchez Delgado, G. Visbal, *Curr. Pharm. Design* 2021, **27**, 1763-1789.
23. C. Viegas-Junior, A. Danuello, V. da Silva Bolzani, E. J. Barreiro, C. A. Manssour Fraga, *Cur. Med. Chem.* 2007, **14**, 1829-1852.
24. D. Gibson, *J. Inorg. Biochem.* 2019, **191**, 77–84.
25. R. G. Kenny, C. J. Marmion, *Chem. Rev.* 2019, **119**, 1058−1137.

26. G. Gasser, I. Ott, N. Metzler-Nolte, *J. Med. Chem*. 2011, **54**, 3-25.

27. R. Alberto, R. Schibli, R. Waibel, U. Abram, A. P. Schubiger, *Coord. Chem. Rev.* 1999, **190–192**, 901-919.

28. C.C. Konkankit, S. C. Marker, K. M. Knopf, J. J. Wilson, *Dalton Trans*. 2018, **47**, 9934-9974.

29. S. Hostachy, C. Policar, N. Delsuc, *Coord. Chem. Rev*. 2017, **351**, 172–188.

30. A. Leonidova, G. Gasser, *ACS Chem. Biol*. 2014, **9**, 2180-2193.

31. E. B. Bauer, A.A. Haase, R. M. Reich, D. C. Crans, F.E. Kühn, *Coord. Chem. Rev.* 2019, **393**, 79-117.

32. P.M. Toro, F. Peralta, J. Oyarzo, S.R. Wilkinson,M. Zavala, R. Arancibia, M. Moncada-Basualto, I. Brito, J. Cisterna, A.H. Klahn, C. López, *J. Inorg. Biochem*. 2021, **219**, 111428. doi: 10.1016/j.jinorgbio.2021.111428

33. I. Machado, S. Fernández, L. Becco, B. Garat, J. S. Gancheff, A. Rey, D. Gambino, *J. Coord. Chem.* 2014, **67**, 1835-1850.

34. E. Rodríguez, I. Machado, B. Rodríguez, M. Lapier, M. C. Zúñiga, J. D. Maya, C. Olea Azar, L. Otero, D. Gambino, *J. Inorg. Biochem*. 2017, **170**, 125-133.

35. A. Bencini, V. Lippolis*, Coord. Chem. Rev.* 2010, **254**, 2096–2180.

36. G. Scalese, J. Benítez, S. Rostán, I. Correia, L. Bradford, M. Vieites, L. Minini, A. Merlino, E. L. Coitiño, E. Birriel, J. Varela, H. Cerecetto, M. González, J. Costa Pessoa, D. Gambino, *J. Inorg. Biochem.* 2015, **147**, 116–125.

37. J. Benítez, L. Guggeri, I. Tomaz, G. Arrambide, M. Navarro, J. Costa Pessoa, B. Garat, D. Gambino, *J. Inorg. Biochem.* 2009, **103**, 609–616.

38. G. I. Lepesheva, L. Friggeri, R. Waterman, *Parasitology* 2018, **145**, 1820-1836.

39. E. Rodríguez, C. Sarniguet, T.S. Moraes, M. Vieites, A.I. Tomaz, A. Medeiros, M.A. Comini, J. Varela, H. Cerecetto, M. González, F, Marques, M.H. García, L. Otero, D. Gambino, *J. Coord. Chem.* 2015, **68**, 2923-2937.

40. R. Rubbiani, T. Weil, N. Tocci, L. Mastrobuoni, S. Jeger, M. Moretto, J. Ng, Y. Lin J. Hess, S. Ferrari, A. Kaech, L. Young, J. Spencer, A. L. Moore, K. Cariou, R. Giorgia, L. Romani, M. Pariano, G. Gasser, *RSC Chem. Biol.* 2021, **2**, 1263-1273.

41. P. V. Simpson, C. Nagel, H. Bruhn, U. Schatzschneider, *Organometallics* 2015, **34**, 3809-3815.

42. S. S. Mendes, J. Marques, E. Mesterházy, J. Straetener, M. Arts, T. Pissarro, J. Reginold, A. Berscheid, J. Bornikoel, R. M. Kluj, C. Mayer, F. Oesterhelt, S. Friaes, B. Royo, T. Schneider, H. Brötz-Oesterhelt, C. C. Romao, L. M. Saraiva, *ACS BioMedChem Au* 2022, **2**, 419–436.

43. M. Soba, G. Scalese, L. Pérez-Díaz, D. Gambino, I. Machado, *Talanta* 2022, **244**, 123413.

44. I. Maisuls, E. Wolcan, O.E. Piro, G.A. Etcheverría, G. Petroselli, R. Erra-Ballsels, F.M. Cabrerizo, G.T. Ruiz, *Dalton Trans.* 2015, **44**, 17064–17074.

45. CrysAlisPro, Oxford Diffraction Ltd., version 1.171.33.48 (release 15-09-2009 CrysAlis171.NET).

46. G. M. Sheldrick, *Acta Crystallogr. A* 2015, **71**, 3–8.

47. G. M. Sheldrick, *Acta Crystallogr. A* 2008, **64**, 112-122.

48. P. Van der Sluis, A. L. Spek, *Acta Crystallogr. A* 1999, **46**, 194-201.

49. A. L. Spek, PLATON, A Multipurpose Crystallographic Tool, Utrecht University, Utrecht, The Netherlands, 1998.

50. S. Keller, Y.C. Ong, Y. Lin, K. Cariou, G. Gasser, *J. Organomet. Chem.* 2020, **906**, 121059. https://doi.org/10.1016/j.jorganchem.2019.121059.

51. P.A. Castelo Teixeira, R. Alves De Castro, F. Rodrigues Lanzana Ferreira, M.M. Lyra Cunha, A. Pérez Torres, C.V. Loureiro Y. Penha, S. Rozental, L.M. Lopes-Bezerra, *Med. Mycol.* 2010, **48**, 687–695.

52. F. Rivas, A. Medeiros, C. Quiroga, D. Benítez, M. Comini, E. Rodríguez-Arce, I. Machado, H. Cerecetto, D. Gambino, *Dalton Trans.* 2021, **50**, 1651–1665.

53. C.M. Du, K. Valko, C. Bevan, D. Reynolds, M.H. Abraham, *Anal. Chem*. 1998, **70**, 4228–4234.

54. L. Ayouni, G. Cazorla, D. Chaillou, B. Herbreteau, S. Rudaz, P. Lantéri, P.A. Carrupt, *Chromatographia* 2005, **62**, 251–255.

55. J.C. Chen, S.G. Weber, *J. Chromatogr*. 1982, **248**, 434–440.

56. J. Karges, S. Kuang, Y. C. Ong, H. Chao, G. Gasser, *Chem. Eur. J.* 2021, **27**, 362 – 370.

57. L.M. MacLean, J. Thomas, M.D. Lewis, I. Cotillo, D.W. Gray, M. De Rycker, *PLoS Negl. Trop. Dis.* 2018, **12**, e0006612, doi:10.1371/journal.pntd.0006612.

58. G.A. Duran-Rehbein, J.C. Vargas-Zambrano, A. Cuellar, C.J. Puerta, J.M. Gonzalez, *Parasite* 2014, **21**, 38, doi:10.1051/parasite/2014040.

59. G. Scalese, I. Machado, I. Correia, J.C. Pessoa, L. Bilbao, L. Pérez-Diaz, D. Gambino, New J. Chem. 2019, **43**, 17756-17773, doi:10.1039/c9nj02589h.

60. M. Vieites, P. Smircich, B. Parajon-Costa, J. Rodriguez, V. Galaz, C. Olea-Azar, L. Otero, G. Aguirre, H. Cerecetto, M. Gonzalez, A. Gómez-Barrio, B. Garat, D. Gambino. J. Biol. Inorg. Chem. 2008, **13**, 723-735, doi:10.1007/s00775-008-0358-7.

61. G. Scalese, I. Machado, G. Salinas, L. Pérez-Díaz, D. Gambino, *Molecules* **2021**, 26, 5375. https://doi.org/10.3390/molecules26175375

62. J.K. Barton, J.M. Goldberg, Ch.V. Kumar, N.J. Turro, *J. Am. Chem. Soc.* 1986, **108**, 2081–2088.

63. A. Santos, I. Ferreira, C. Pinheiro, V. Santos, M. Lopes, L. Teixeira, W. Rocha, G. Rodrigues, H. Beraldo, *ACS Omega* 2018, **3**, 7027–7035.

64. A. Gerpe, G. Álvarez, D. Benítez, L. Boiani, M. Quiroga, P. Hernández, M. Sortino, S. Zacchino, M. González, H. Cerecetto, *Bioorg. Med. Chem.* 2009, **17**, 7500–7509.

65. M. Santivañez-Veliza, E. Moreno-Viguri, S. Pérez-Silanes, J. Varela, H. Cerecetto, M. González, E. Lizarraga, *J. Chromatogr. B* 2017, **1061–1062**, 225–232.

66. S.C. Bindu Bavisetty, B. Narayan, *J. Food Sci. Technol*. 2015, **52**, 6083–6089.

67. E. G. Lewars, in *Computational Chemistry: Introduction to the Theory and Applications of Molecular and Quantum Mechanics*, Springer International Publishing, Cham, 2016, DOI: 10.1007/978-3-319-30916-3_4, pp. 101-191.

68. M. J. Frisch, G. W. Trucks, H. B. Schlegel, G. E. Scuseria, M. A. Robb, J. R. Cheeseman, G. Scalmani, V. Barone, B. Mennucci, G. A. Petersson, H. Nakatsuji, M. Caricato, X. Li, H. P. Hratchian, A. F. Izmaylov, J. Bloino, G. Zheng, J. L. Sonnenberg, M. Hada, M. Ehara, K. Toyota, R. Fukuda, J. Hasegawa, M. Ishida, T. Nakajima, Y. Honda, O. Kitao, H. Nakai, T. Vreven, J. Montgomery, J. E. Peralta, F. Ogliaro, M. J. Bearpark, J. Heyd, E. N. Brothers, K. N. Kudin, V. N. Staroverov, R. Kobayashi, J. Normand, K. Raghavachari, A. P. Rendell, J. C. Burant, S. S. Iyengar, J. Tomasi, M. Cossi, N. Rega, N. J. Millam, M. Klene, J. E. Knox, J. B. Cross, V. Bakken, C. Adamo, J. Jaramillo, R. Gomperts, R. E.

Stratmann, O. Yazyev, A. J. Austin, R. Cammi, C. Pomelli, J. W. Ochterski, R. L. Martin, K. Morokuma, V. G. Zakrzewski, G. A. Voth, P. Salvador, J. J. Dannenberg, S. Dapprich, A. D. Daniels, Ö. Farkas, J. B. Foresman, J. V. Ortiz, J. Cioslowski and D. J. Fox, Gaussian 09, 2009, Gaussian, Inc.

69. W. R. Wadt, P. J. Hay, *J. Chem. Phys.* 1985, **82**, 284-298.
70. A. V. Marenich, C. J. Cramer and D. G. Truhlar, *J. Phys. Chem. B* 2009, **113**, 6378-6396.
71. G. Jones, P. Willett, R.C. Glen, A.R. Leach, R. Taylor, *J. Mol. Biol.* 1997, **267**,727-748.
72. H.M. Berman, J. Westbrook, Z. Feng, G. Gilliland, T.N. Bhat, H. Weissig, I.N. Shindyalov, P.E. Bourne, *Nucleic Acids Res.* 2000, **28**, 235-242.
73. P. Labute, Protonate3D: Assignment of ionization states and hydrogen coordinates to macromolecular structures, *Proteins: Struct. Funct. Bioinform.* 2009, **75**, 187-205.
74. P. Labute, Molecular Operating Environment (MOE), Chemical Computing Group Inc., 1010 Sherbooke St. West, Suite #910, Montreal, QC, Canada, H3A 2R7, 2014.
75. C.A. Baxter, C.W. Murray, D.E. Clark, D.R. Westhead, M.D. Eldrige, *Proteins: Struct. Funct. Genet.* 1998, **33**, 367-382.
76. M.D. Eldrige, C.W. Murray, T.R. Auton, G.V. Paolini, R.P. Mee, *J. Comput. Aided Mol. Des.* 1997, **11**, 425-445.
77. Discovery Studio Visualizer v2.5.5.9350, Copyright 2005-2009, Accelrys Software Inc.
78. V. P. Fadeeva, V. D. Tikhova, O. N. Nikulicheva, *J. Anal. Chem.* 2008, **63**, 1094–1106.

79. A. Martínez, T. Carreon, E. Iniguez, A. Anzellotti, A. Sánchez, M. Tyan, A. Sattler, L. Herrera, R.A. Maldonado, R.A. Sánchez-Delgado, *J. Med. Chem*. 2012, **55**, 3867-3877.

80. R.A. Sánchez-Delgado, M. Navarro, K. Lazardi, R. Atencio, M. Capparelli, F. Vargas, J. A.Urbina, A. Bouillez, A. F.Noels, D. Masi, *Inorganica Chim. Acta* 1998*,* **275-276***,* 528–540*.*

81. S. Betanzos-Lara, C. Gómez-Ruiz, L.R. Barrón-Sosa, I. Gracia-Mora, M. Flores-Álamo, N. Barba-Behrens, *J. Inorg. Biochem*. 2012, **114**, 82-93.

82. S.S. Singh, *Z. Naturforsch. A* 1969, **24**, 2015–2016.

83. R.C. Van der Drift, J.W. Sprengers, E. Bouwman, W.P. Mul, H. Kooijman, A.L. Spek, E. Drent, *Eur. J. Inorg. Chem.* 2002, **8**, 2147–2155.

84. X. Li, D. Zhang, G. Lu, G. Xiao, H. Chi, Y. Dong, Z. Zhang, Z. Hu, *J. Photochem. Photobiol. A: Chem*. 2012, 241, 1-7.

85. A.M. Heyns, *Spectrochim. Acta Part A, Mol. Spectros*. 1977, **33**, 315–322.

86. L.J. Farrugia, *J. Appl. Cryst.* 1997, **30**, 565.

87. T.N. Thompson, T.N. *Med. Res. Rev*. 2001, **21**, 412–449.

88. M. Starek, A. Plenis, M. Zagrobelna, M. Dąbrowska, Pharmaceutics 2021, **13**, 440.

89. X. Liu, B. Testa, A. Fahr, Pharm. Res. 2010, **28**, 962–977.

90. E. Kerns, L. Di, Drug-Like Properties: Concept, Structure Design and Methods, From ADME to Toxicity Optimization. Chapter 5 Lipophilicity Pag. 39-49, 10.1016/B978-012369520-8.50003-6, 2008.

91. H. Van De Waterbeemd, R. Mannhold, Lipophilicity in drug action and toxicology. In Methods and Principles in Medicinal Chemistry, V. Pliska, B.

Testa, H. Van De Waterbeemd, Eds.; VCH Publishers: Weinheim, Germany, 1996.

92. E.C. Bate-Smith, R.G. Westall, *Biochim. Biophys. Acta* 1950, **4**, 427–440.

93. D. Naumann, *Appl. Spectrosc. Rev.* 2001, **36**, 239-298.

94. C.Yu, E. Gestl, K. Eckert, D. Allara, J.Irudayaraj, *Cancer Detect. Prev.* 2006, **30**, 515-522.

95. K.W. Short, S. Carpenter, J.P. Frever, J. R. Mourant, *Biophys. J.* 2005, **88**, 4274-4288.

96. M. Sirajuddin, S. Ali, A. Badshah, *J. Photochem. Photobiol. B: Biology* 2013, **124**, 1-19.

97. F. Rivas, C. Del Mármol, G. Scalese, L. Pérez-Díaz, I. Machado, O. Blacque, A. Medeiros, M. Comini, D. Gambino, *J. Inorg. Biochem.* 2022, **237**, 112016. https://doi.org/10.1016/j.jinorgbio.2022.112016

98. F.S. Bucknera, J.A.Urbina, *Int. J. Parasitol.-Drugs* 2012, **2**, 236–242.

99. A.E. Muñiz. Pediatric. In: Emergency Medicine. Chapter 126 - Other Important Rashes 2008, 880–897.

100. C-K Chen, S. S. F. Leung, C. Guilbert, M. P. Jacobson, J. H. McKerrow, L. M. Podust, *PLOS Negl. Trop. Dis.* 2010, https://doi.org/10.1371/journal.pntd.0000651